Thermal droop in III-nitride based light-emitting diodes: Physical origin and perspectives 🅕

🆔 **Matteo Meneghini,** 🆔 **Carlo De Santi,** 🆔 **Alberto Tibaldi, et al.**

COLLECTIONS

🅕   This paper was selected as Featured

View Online   Export Citation   CrossMark

ARTICLES YOU MAY BE INTERESTED IN

Thermal droop in III-nitride based light-emitting diodes: Physical origin and perspectives Ⓕ

Matteo Meneghini,[1,a] Ⓘ Carlo De Santi,[1] Ⓘ Alberto Tibaldi,[2,3] Ⓘ Marco Vallone,[2] Ⓘ Francesco Bertazzi,[2,3] Ⓘ Gaudenzio Meneghesso,[1] Ⓘ Enrico Zanoni,[1] Ⓘ and Michele Goano[2,3] Ⓘ

AFFILIATIONS

[1] Department of Information Engineering, University of Padova, via Gradenigo 6/b, 35131 Padova, Italy
[2] Department of Electronics and Telecommunications, Politecnico di Torino, corso Duca degli Abruzzi 24, 10129 Turin, Italy
[3] Consiglio Nazionale delle Ricerche (CNR), Istituto di Elettronica e di Ingegneria dell'Informazione e delle Telecomunicazioni (IEIIT), corso Duca degli Abruzzi 24, 10129 Turin, Italy

[a] Author to whom correspondence should be addressed: matteo.meneghini@dei.unipd.it

ABSTRACT

This tutorial paper focuses on the physical origin of thermal droop, i.e., the decrease in the luminescence of light-emitting diodes (LEDs) induced by increasing temperature. III-nitride-based LEDs are becoming a pervasive technology, covering several fields from lighting to displays, from automotive to portable electronics, and from horticulture to sensing. In all these environments, high efficiency is a fundamental requirement, for reducing power consumption and system cost. Over the last decade, a great deal of effort has been put in the analysis of the efficiency droop, the decrease in LED internal quantum efficiency (IQE) induced by high current density. On the other hand, an IQE decrease is observed also for increasing temperature, a phenomenon usually referred to as thermal droop. For commercial LEDs, the IQE decrease related to thermal droop can be comparable to that of efficiency droop: for this reason, understanding thermal droop is a fundamental step for making LEDs capable of operating at high temperature levels. In several fields (including street lighting, automotive, photochemical treatments, projection, entertainment lighting, etc.), compact and high-flux light sources are required: typically, to reduce the size, weight, and cost of the systems, LEDs are mounted in compact arrays, and heat sinks are reduced to a minimum. As a consequence, LEDs can easily reach junction temperatures above 85–100 °C and are rated for junction temperatures up to 150–175 °C (figures from commercially available LED datasheets: Cree XHP70, Osram LUW HWQP, Nichia NVSL219CT, Samsung LH351B, and LedEngin LZP-00CW0R) and this motivates a careful analysis of thermal droop. This paper discusses the possible physical causes of thermal droop. After an introduction on the loss mechanisms in junctions, we will individually focus on the following processes: (i) Shockley–Read–Hall (SRH) recombination and properties of the related defects; (ii) Auger recombination and its temperature dependence, including the discussion of trap-assisted Auger recombination; (iii) impact of carrier transport on the thermal droop, including a discussion on carrier delocalization, escape, and freeze out; (iv) non-SRH defect-related droop mechanisms. In addition, (v) we discuss the processes that contribute to light emission at extremely low current levels and (vi) the thermal droop in deep ultraviolet LEDs, also with reference to the main parasitic emission bands. The results presented within this paper give a tutorial perspective on thermal droop; in addition, they suggest a pathway for the mitigation of this process and for the development of LEDs with stable optical output over a broad temperature range.

TABLE OF CONTENTS

I. INTRODUCTION

Since the fabrication of the first blue LED, a continuous research work has been carried out by the scientific community, with the final goal of increasing the quantum efficiency from less than 1% internal quantum efficiency (IQE) of the early days[2] to more than 90% demonstrated more recently.[3] Such an improvement has been possible thanks to the optimization of material properties and of device structure; nevertheless, the most relevant changes have been achieved thanks to the ever-increasing understanding of the physics of III-nitride LEDs.

Compared to conventional semiconductors, GaN has several characteristics that were initially considered to be detrimental for reaching efficient light emission. First, a high dislocation density (up to $10^8 \, cm^{-2}$) results from the heteroepitaxial growth on foreign substrates, such as Al_2O_3 and SiC. Dislocations may act as dark spots, as reported in previous publications,[4,5] but the overall performance of state-of-the-art GaN LEDs (threading dislocation density $<10^8 \, cm^{-2}$) is only slightly affected by dislocation density,[6,7] thanks to the existence of localization effects,[8–10] that are discussed in detail in Sec. III D 1. c-plane LEDs are typically based on strained InGaN quantum wells (QWs), where polarization-induced fields create a strong

quantum-confined Stark effect (QCSE) [see a schematic representation in Fig. 1(a)]. Such a polarization field can be higher than 1 MV/cm,[11] thus inducing a strong bending of the band diagram in InGaN quantum wells. This has three direct consequences on the optical properties of InGaN LEDs, namely, a redshift of the peak emission energy; a reduction in the oscillator strength, due to a decrease in the spatial overlap of the electron and hole wavefunctions; and a strong dependence of the emission wavelength on the excitation intensity (blueshift with increasing carrier density), due to the Coulomb screening of the internal fields.

Over the years, thanks to the significant efforts of the scientific community and to a substantial investment of the industrial players, it has been demonstrated that the issues described above are not fundamental limits of III-nitride LEDs but scientific problems that can be overcome through a careful optimization of device structure and fabrication process. Nowadays, it is possible to fabricate InGaN LEDs having high internal quantum efficiency, and this has cleared the way for a massive market penetration of LEDs in several fields.

Unfortunately, the IQE of InGaN LEDs is not constant but has a strong dependence on current and carrier density. A typical IQE vs carrier density curve is shown in Fig. 1(b): at low current levels, efficiency is limited by the existence of Shockley–Read–Hall (SRH) recombination (whose coefficient is typically labeled A), while at high carrier densities, higher order mechanisms (including Auger recombination, with coefficient C, and carrier leakage) come into play.[3,12]

In the past decade, a great deal of attention has been focused on the study and analysis of the efficiency droop, i.e., the decrease of IQE at high carrier densities.[13–15] Typically, LEDs reach peak efficiency at relatively low current density (current for peak efficiency, I_{peak}, is in the range of 1–10 A/cm^2), well below the operating current density ($I_{nom} = 35–100$ A/cm^2).[16–21] The efficiency droop may account for a 20%–30% decrease in quantum efficiency, by moving from I_{peak} to I_{nom}.[16,17,20–22] A schematic representation of efficiency droop is given in Fig. 2 (left): at high current density, high-order recombination/leakage processes lead to a drop in internal quantum efficiency. For simplicity, in this figure, we only consider the effect of one dominant process, Auger recombination. The results in the figure show that with an increasing Auger rate, the
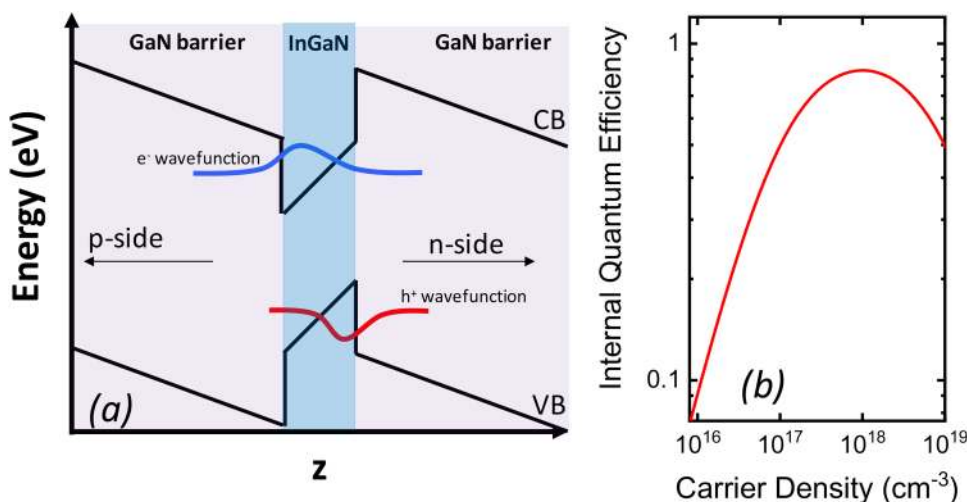
FIG. 1. (a) Schematic representation of the effect of polarization fields on the band bending in an InGaN quantum well with GaN barriers. The spatial separation of electron and hole wavefunctions is also shown. (b) Calculated dependence of internal quantum efficiency on carrier density (for calculations, the simplified ABC model with recombination coefficients $A = 10^5 \, s^{-1}$, $B = 10^{-12} \, cm^3 \, s^{-1}$, and $C = 10^{-31} \, cm^6 \, s^{-1}$ were used; such an oversimplified approach is used for illustration purposes).
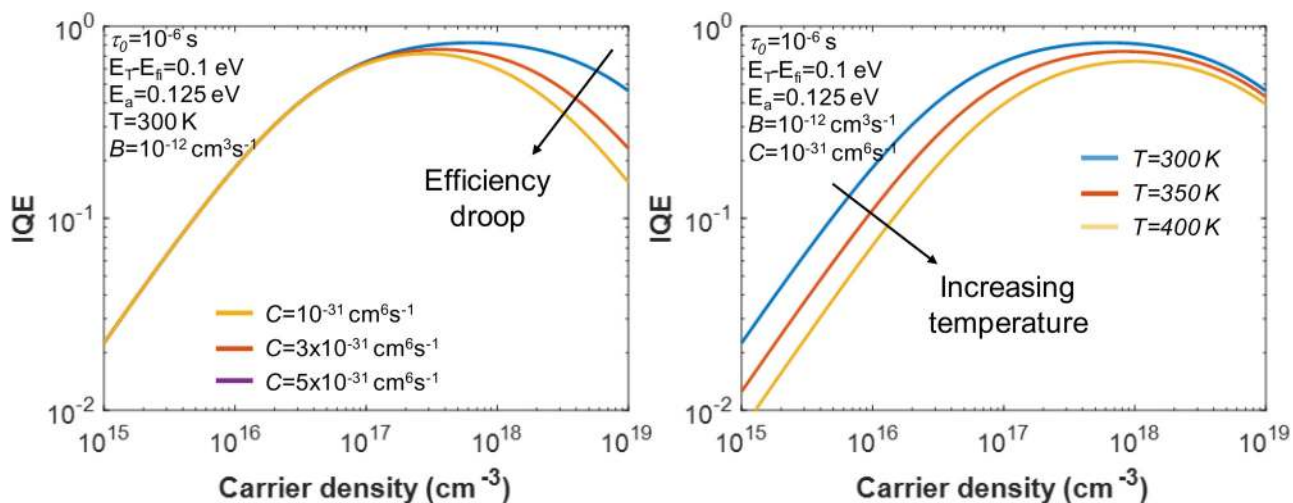
FIG. 2. Simplified representation (for illustration purposes) of the impact of (left, for T = 300 K) efficiency droop and (right) thermal droop on the internal quantum efficiency of LEDs. For simplicity, in this figure, we consider one dominant mechanism (Auger recombination), as responsible for efficiency droop, and we describe the effect of increasing Auger coefficient on the IQE characteristics. For both figures, we consider two temperature-dependent mechanisms, namely, SRH recombination [involving defects located at $E_T - E_{Fi}$ = 0.1 eV, with $\tau_0 = 10^{-6}$ s, see Eq. (5)], and a dominant escape process with energy barrier equal to 0.125 eV [see Eq. (13) and Ref. 116]. The bimolecular recombination coefficient is $B = 10^{-12}$ cm^{-3} s^{-1}. Other processes come into play and are described in detail in the paper.

efficiency can substantially decrease in the high current region, while remaining almost unaffected at low current levels.

The efficiency of state-of-the-art LEDs may be limited also by thermal droop, which is a decrease in the IQE induced by operation at high temperatures.[22–25] A schematic representation of thermal droop is given in Fig. 2 (right): at high temperatures, the increase in parasitic recombination and leakage processes leads to a drop in internal quantum efficiency. For simplicity, in this figure, we only consider the effect of two mechanisms, namely, SRH recombination [involving defects located at $E_T - E_{Fi}$ = 0.1 eV, with $\tau_0 = 10^{-6}$ s, see Eq. (5)] and a dominant escape process with energy barrier equal to 0.125 eV [see Eq. (13) and Ref. 26]. For both figures, we used $B = 10^{-12}$ cm^{-3} s^{-1}. The results in the figure show that with increasing temperature, the larger SRH and escape rates can lead to a substantial decrease in the efficiency. The effect observed in the low carrier density region is mostly ascribed to the increased SRH recombination, whereas the drop observed in the high carrier density regime is related to the increasing escape rate. In the following, we will discuss the physical origin of thermal droop and show that with increasing temperature, several processes may affect the efficiency of LEDs, both in the low and in the high current regime.

Despite its importance, thermal droop has not been studied with the same intensity as the efficiency droop, although its impact on IQE is of comparable magnitude. For reference, one can consider that commercially available LEDs can show a >20% IQE decrease, when junction temperature is increased from 25 °C to 150 °C, at nominal current levels (see, for instance, Ref. 27). This temperature range is often within the absolute maximum ratings, thus being representative of realistic operating conditions.

Several end users want to minimize the number of LEDs for achieving a given luminous flux in their products, with the aim of

minimizing the cost, weight, and size of light sources. As representative examples, we mention here the use of compact arrays of LEDs in automotive headlights, projection systems, illuminators for photochemical treatments, and street lamps. In all these fields, lightweight and/or compact illuminators are required, and this has direct consequences on the self-heating of the devices. In several applications, LEDs can operate at temperatures higher than 85–100 °C, and for this reason, several manufactures give the specifications at 85 °C in the datasheet and rate them up to 150–175 °C.[1] In these conditions, thermal droop may become relevant, and for this reason the related processes need to be studied in detail. Understanding and minimizing efficiency droop and thermal droop will allow us to further increase device performance in real-life applications.

Several papers and book chapters have been presented on the efficiency droop, but only a few systematic analyses of thermal droop can be found in the literature. The aim of this paper is to review the most relevant processes responsible for the thermal droop in III-nitride based LEDs; we will focus mostly on InGaN-based devices, but we will present also some recent data obtained on AlGaN UV diodes and on red and infrared material systems, to help the reader having a comprehensive view on the topic.

The paper is organized as follows: first, we will summarize the most relevant loss mechanisms that limit the IQE of III-nitride based LEDs. Then, we will analyze one by one the dominant processes responsible for thermal droop, with specific reference to Shockley–Read–Hall (SRH) recombination, Auger recombination, carrier transport and escape, carrier freeze out, and non-SRH defect-related droop mechanisms. Finally, for completeness, we describe the processes that contribute to light emission at extremely low current levels, and the thermal droop in
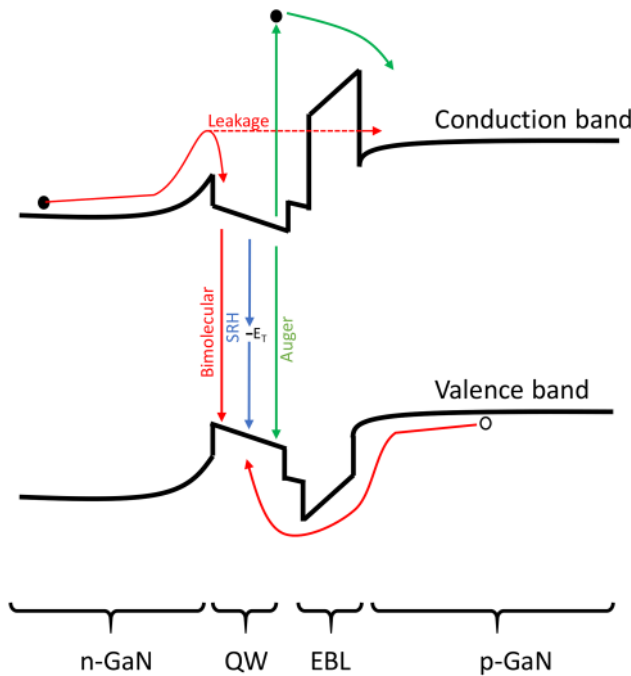
FIG. 3. Schematic band diagram of a single-quantum-well LED, indicating the dominant loss mechanisms that limit the IQE: SRH recombination, Auger recombination, and carrier leakage.

deep ultraviolet (DUV) LEDs, including the contribution on the main parasitic emission bands.

II. MECHANISMS LIMITING THE EFFICIENCY OF III-NITRIDE-BASED LEDS

Figure 3 shows a schematic band diagram of a single-quantum-well LED. The quantum well is based on InGaN, while the barriers and n-type material are made of GaN. Between the
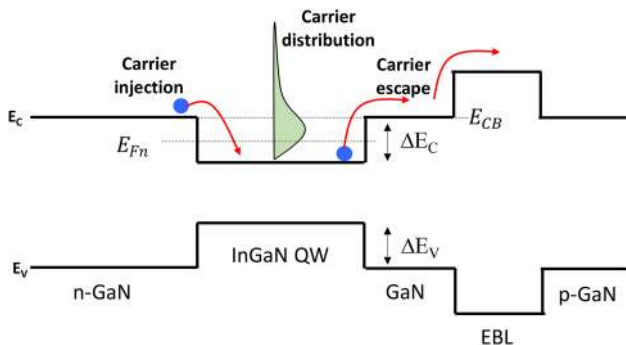

FIG. 4. Schematic band diagram of a single-quantum-well LED, focusing on the carrier injection and escape processes.

QW and the p-type material, an AlGaN electron blocking layer (EBL) is present. The efficiency of such a simple device can be limited by several factors.

A. Injection efficiency and carrier leakage

First, one needs to consider that only a fraction of the electrons crossing the junction are effectively captured by the quantum well.[28] The remaining part can transfer to the p-side either via leakage through/over the EBL[29] or through defect-related paths,[30] depending on the current level and on the device structure. The existence of carrier leakage phenomena is typically taken into account by the injection efficiency η_{inj}, a parameter that describes the fraction of bias current that generates carriers in the quantum well region.[31]

In a double heterostructure, carriers in the recombination region are distributed according to the Fermi–Dirac statistics. In quantum wells, the energy levels are quantized, and electrons mostly reside in the ground state, but a part of the carriers may have enough energy to escape from the active region, as shown in Fig. 4. In this case, the parameter that controls the escape is the conduction/valence band discontinuity $\Delta E_C / \Delta E_V$. In a classical approximation, for a heterostructure, the fraction of carriers with energy higher than the barrier can be calculated as

$$n_{leak} \int_{E_{C,B}}^{\infty} \rho f_{FD}(E) dE, \tag{1}$$

where $E_{C,B}$ is the conduction band energy of the barrier, ρ is the density of states, and f_{FD} is the Fermi–Dirac distribution.[32] This gives an exponential function that depends on the energy distance between the Fermi level and $E_{C,B}$ [$\sim \exp^{(E_{Fn} - E_{C,B})/k_B T}$]. For InGaN quantum wells, the escape from the well to the barrier has been modeled according to the thermionic emission model,[33,34] by using the following equation:

$$J = q n_{c,v} \left(\frac{kT}{2\pi m^\star} \right) \exp\left(-\frac{\Delta E}{k_B T} \right), \tag{2}$$

where $n_{c,v}$ is the carrier density in the well, ΔE is the potential barrier at the well/barrier interface, and $m^\star$ is the effective mass.[34] Ikeda et al.[34] indicated that thermionic emission current can be suppressed when barrier height becomes larger than $\sim k_B T$. A second consideration is that—for the same barrier height—the thermionic current of electrons is higher than that of holes due to the lighter effective mass of electrons ($m_e = 0.2\, m_0$ and $m_h = 0.8\, m_0$).

Vampola et al.[35] were able to experimentally demonstrate the presence of electron overflow in InGaN-based LEDs, under typical bias conditions. To this aim, they grew a LED structure with an extra quantum well located beyond the electron blocking layer, at the p-side. Such a quantum well has a lower indium content with respect to the main QW of the devices, thus giving shorter wavelength emission. The presence of overflow was demonstrated by the detection of short wavelength luminescence at high current levels. The authors noted that, besides the traditional overflow process, Auger recombination may contribute to carrier overflow. In fact, Auger-generated electrons have a significant probability of leaking above the EBL and

reaching the extra quantum well located on the p-side. This is in agreement with later studies on the topic,[36] reporting the detection of Auger electrons by electron emission spectroscopy; the appearance of high energy electron peaks was ascribed to the generation of hot electrons in the InGaN quantum wells by an Auger process.

B. Shockley–Read–Hall recombination

Once carriers reach the active region, they can either recombine or escape out of the quantum well. Three main recombination paths are typically considered. At low current densities, Shockley–Read–Hall recombination[37,38] plays an important role: the recombination dynamics can be described (in an over-simplified approach) through the ABC model that takes into account the rates of the dominant (bimolecular, Auger, and SRH) recombination processes, by defining the internal quantum efficiency as $Bn^2/(An + Bn^2 + Cn^3)$. Here A, B, and C are the SRH, bimolecular, and Auger recombination coefficients described in this section and n is the carrier density. As can be easily understood by looking at the denominator, at low carrier densities, the efficiency is mainly limited by the lowest order term An, i.e., by the SRH recombination rate. To be more specific, we consider that the presence of defects within the active region can promote defect-assisted non-radiative recombination, thus leading to a decrease in the internal quantum efficiency.[39] The net SRH recombination rate can be approximated as[32]

$$R_{\text{SRH}} \approx \frac{np - n_i^2}{\tau_p\left[n + n_i\exp\left(\dfrac{E_T - E_{Fi}}{k_BT}\right)\right] + \tau_n\left[p + n_i\exp\left(\dfrac{E_{Fi} - E_T}{k_BT}\right)\right]}$$
$$\approx An, \tag{3}$$

where n and p are the electron and hole densities, n_i is the intrinsic carrier concentration, E_{Fi} is the intrinsic Fermi level, E_T is the trap energy level, and $A = (\tau_{\text{SRH}})^{-1}$. The lifetimes τ_n and τ_p depend on several parameters, including the trap density N_T, the thermal carrier velocity v_{th}, and the capture cross section of defects σ,

$$1/\tau_p = N_T\sigma_p v_{\text{th},p}, \quad 1/\tau_n = N_T\sigma_n v_{\text{th},n}. \tag{4}$$

In doped semiconductors, the SRH recombination rate is limited by the capture of minority carriers. Since the lifetimes τ_n and τ_p are inversely proportional to the trap densities, a reduction in the concentration of defects is necessary for achieving high efficiency. The energetic position of defects also plays a fundamental role in defining how efficient a defect is in capturing carriers: under the assumption of identical capture rates for electrons and holes, in an intrinsic material, the lifetime for SRH recombination becomes[40]

$$\tau_{\text{intrinsic}} = \tau_0\left[1 + \cosh\left(\frac{E_T - E_{Fi}}{k_BT}\right)\right]. \tag{5}$$

Since E_{Fi} is typically near the midgap, the most efficient SRH recombination centers are those located near the midgap.

Typically, SRH recombination impacts on the IQE curve in the low current region;[40] at low current injection, linearity of optical power vs current curve is lost, and the trend is quadratic. This can be particularly detrimental for display applications, where LEDs need to be dimmed to very low power levels. A non-uniform light distribution can arise from the different defect densities present in the individual LEDs arranged in a matrix.

Considering the wide bandgap of GaN (3.4 eV), midgap defects are very deep (1.7 eV) with respect to the conduction band edge. Optical spectroscopy techniques are often necessary to identify these traps and to study their impact on SRH recombination.[41] To have a feeling on realistic values of the A coefficient, one can look into a recent paper[17] that reported values of the SRH recombination coefficient in the range between $6 \times 10^4\,\text{s}^{-1}$ and $2 \times 10^6\,\text{s}^{-1}$. It is worth noticing that higher values have also been reported; see, for instance, Ref. 42 and references therein.

Recently, the interest on the physical origin of Shockley–Read–Hall recombination in GaN-based LEDs has significantly increased. Several groups investigated the characteristics of the defects involved in SRH recombination. Meneghini et al.[43] demonstrated that LEDs with higher SRH recombination coefficients have effectively a higher density of traps (Fig. 5), which can be detected by deep-level transient spectroscopy measurements. They suggested that the traps can be related to native defects, such as nitrogen-related defects or vacancies.

Dreyer et al.[44] used first-principles calculations to estimate the transition levels and capture coefficients of several V_{Ga} complexes, namely V_{Ga}–3H, V_{Ga}–O_N–2H, V_{Ga}–2H, and V_{Ga}–O_N–H. They demonstrated that, depending on the wavelength, concentrations around $10^{16}\,\text{cm}^{-3}$ of these defects can favor SRH recombination, thus severely impacting on the IQE of the devices. Young et al.[45] studied the role of calcium as a possible source of non-radiative
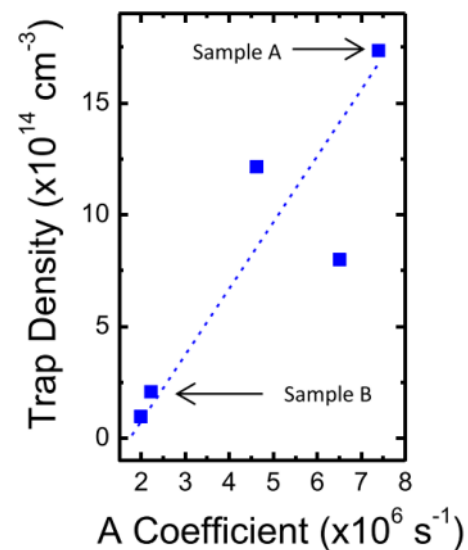
FIG. 5. Relation between trap density and non-radiative recombination coefficient for the individual analyzed devices. Reprinted with permission from Meneghini et al., Appl. Phys. Lett. **104**(11), 113505 (2014). Copyright 2014 AIP Publishing LLC.

recombination in samples grown by molecular beam epitaxy (MBE). They demonstrated an increase in the output power by one order of magnitude, when calcium concentration was reduced in the LED active region, and ascribed this to the role of Ca as a SRH recombination center. Haller *et al.*[46] indicated that for samples with an indium content of 12%, V_{Ga} and related complexes are not supposed to strongly impact on efficiency. They suggested the following mechanism: during growth, nitrogen vacancies (V_N) are created near the surface. Such defects segregate at the surface, due to their higher formation energy in bulk GaN. If indium is present, V_N defects are incorporated in the bulk, due to a decrease in their formation energy in InGaN layers, and this favors SRH recombination. They also suggested that potential candidates such as SRH centers could be complexes of V_N and In[47,48] or divacancy complexes (V_N and V_{III}).[49] As specified above, efficient SRH defects are located near the midgap; in GaN, midgap traps are too deep to ensure an easy detection by conventional techniques such as capacitance deep-level transient spectroscopy (C-DLTS). Recently, the presence of near-midgap defects was detected by techniques based on optical excitation, such as deep-level optical spectroscopy (DLOS) and photocurrent spectroscopy (PCS).[41,50]

At intermediate current densities, close to the peak of the IQE curve, bimolecular (or radiative) recombination processes dominate. The rate of radiative recombination is proportional to the product of electron and hole densities through the *B* coefficient, which depends on the properties of the semiconductor material. For GaN devices, values between $10^{-12}\,cm^3\,s^{-1}$ and $10^{-11}\,cm^3\,s^{-1}$ are often reported, depending on device properties and emission wavelength.[19,51,42]

C. Auger recombination

The third, and more debated, recombination process that takes place in the quantum wells of LEDs is Auger recombination. Belonging to the category of carrier–carrier interactions, Auger recombination is the inverse process of impact ionization. In this process, the energy released by a recombination event is transferred to a third carrier, which is promoted to a high energy state. If the third carrier is an electron, the process is named electron–electron–hole (eeh) Auger recombination; if it is a hole, it is referred to as hole–hole–electron (hhe) Auger recombination. This process becomes relevant at high carrier densities, since the recombination

rate scales with the third power of carrier density, through a coefficient *C* (rate $\sim Cn^2p$ and Cnp^2 for eeh and hhe, respectively).

As for other processes, during Auger recombination, both momentum and energy are conserved. This leads to a threshold kinetic energy for the initiating the Auger process: at energies lower than this threshold, Auger recombination is not possible without the contribution of other scattering mechanisms. Three different Auger processes have been considered for GaN-based LEDs. The first is direct Auger recombination [Fig. 6(a)], where the conservation of energy and momentum is ensured without the involvement of additional players (e.g., phonons or traps). Piprek[52] calculated that, when the SRH and *B* coefficients are respectively equal to $10^7\,s^{-1}$ and $2\cdot10^{-11}\,cm^3\,s^{-1}$, only Auger coefficients larger than $10^{-31}\,cm^6\,s^{-1}$ can cause a significant efficiency droop; very similar considerations had been already presented in Ref. 53. Hader *et al.*[54] considered direct Auger processes and simulated their contribution by solving the scattering equations. They demonstrated that direct Auger losses have a negligible impact and presented a fitted value of the Auger coefficient equal to $3.5\cdot10^{-34}\,cm^6\,s^{-1}$. Delaney *et al.*[55] considered both intraband Auger (scattering of electron to the lowest conduction band) and interband Auger, involving scattering to the second-lowest conduction band. They demonstrated that the first process is dominant for In-rich alloys ($E_G < 1.8\,eV$), whereas the second is dominant for alloy concentrations relevant for solid-state lighting ($E_G > 2.2\,eV$). Bertazzi *et al.*[56] studied direct interband and intraband Auger recombination (both eeh and hhe) in bulk InGaN, by the first-order perturbation theory. They showed that the intraband Auger coefficient is negligible for wavelengths relevant in lighting and investigated the resonant enhancement associated with interband transitions in the blue–green range. They calculated a room temperature eeh Auger coefficient around $10^{-32}\,cm^6\,s^{-1}$ at 2.9 eV.

Kioupakis *et al.*[57] showed that the recombination rate due to direct Auger recombination [Fig. 6(a)] is negligible, compared to the phonon- and alloy-scattering assisted terms. They indicated that the impact of indirect Auger processes [Fig. 6(b)] is much stronger than that of direct Auger, and the related coefficient can account for the efficiency droop in nitride LEDs. The indirect Auger process is assisted by a scattering mechanism (electron–phonon coupling, alloy disorder, or defect scattering), which provides additional momentum, thus enabling Auger transitions to a wider range of states[57] [Fig. 6(b)].
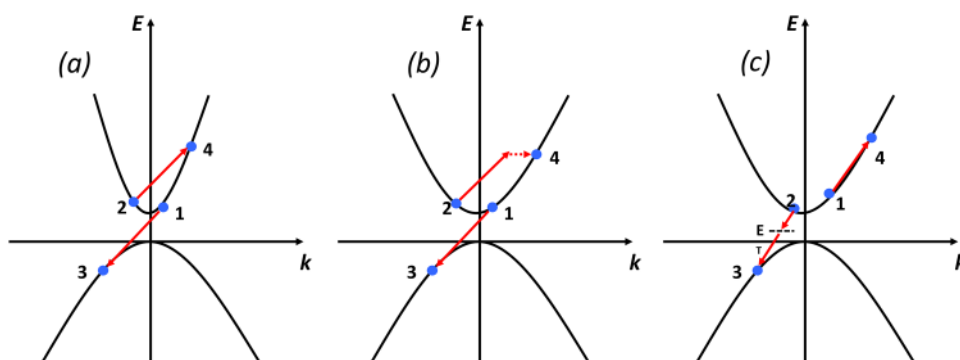

FIG. 6. Schematic representation of Auger recombination processes in InGaN LEDs. (a) Direct Auger recombination. (b) Indirect Auger recombination. (c) eeh Auger recombination where a trap acts as a virtual state.

Recent studies[17,58] suggested that besides the intrinsic Auger processes that are typical for low-defect materials, the presence of SRH centers may foster an additional trap-assisted Auger recombination process (TAAR), which favors droop in highly defective material. The authors of these papers suggested that the TAAR mechanism in Fig. 6(c) may have the right dependence on carrier density to account for such defect-dependent Auger. Specifically, this process consists in Auger scattering involving a trap as a virtual state. Near-midgap defects may reduce the threshold for Auger scattering, thus making these transitions possible. In the literature, values of Auger-like coefficient ranging from $10^{-33}\,\mathrm{cm^6\,s^{-1}}$ to $10^{-30}\,\mathrm{cm^6\,s^{-1}}$ have been reported, depending on the analyzed technology and sample quality (see, for instance, Refs. 17, 52, and 59–61).

D. Other processes that limit IQE

The mechanisms described above are the most investigated loss mechanisms for GaN-based optoelectronic devices. In addition to these, some other processes have been proposed and analyzed for explaining the loss of efficiency of LEDs.

Ryu et al.[62] pointed out that the distribution of carriers in InGaN multi-quantum well (MQW) structures can be inhomogeneous, and this may imply a significant reduction in the effective light-emitting volume. This has been ascribed first to fluctuations in In composition inside the quantum wells, which may lead to localization of electron and holes. A reduction in the active volume may lead to a higher local carrier density, thus favoring high-order loss processes.

A second factor leading to a reduction in the active volume is given by the polarization fields, which lead to non-uniform electron and hole distributions within the quantum wells. For a QW thickness of 2.5–3.0 nm, the effective QW thickness can be reduced to ~1 nm (see Ref. 62 and references therein). A third factor that may lead to non-uniform efficiency is the inefficient transport of holes through the MQW structure. Holes are mostly injected in the quantum well closer to the p-side;[63] this is another factor that limits the volume of the recombination region, thus leading to an increase in the Auger-like non-radiative rate.

Another model proposed as a cause for low LED efficiency is density-activated defect recombination (DADR), as proposed by Hader et al.[64] The idea is that, at low currents, electrons and holes occupy states in local potential minima, which can be generated by fluctuations in well composition or well width. At higher carrier densities, electrons can escape these minima, thus filling the entire quantum well. If potential minima are defect free and separated from defective regions, DADR occurs only at high current levels, once carriers exit the potential minima.

At high current densities, phase-space filling (PSF) has also been predicted by Hader et al.[65] to significantly contribute to the recombination rates. David and Grundmann[19] investigated this aspect by means of differential carrier lifetime measurements. They demonstrated that the optical characteristics can be fitted by an ABC model, which takes into account PSF: in this way, they were able to explain the shortening of both radiative and non-radiative lifetimes with increasing current. They explained that the radiative recombination rate follows Bn^2 only at low carrier densities, where the electron and hole distributions are Boltzmann-like. At higher carrier densities (degenerate regime), radiative recombination becomes monomolecular, i.e., proportional to n.

Auf der Maur et al.[66] investigated the losses related to random alloy fluctuations, which are naturally present in InGaN alloys. To calculate quantitatively the impact of alloy fluctuations on LED efficiency, they calculated the spontaneous emission properties of single-quantum-well (SQW) LEDs with indium concentrations between 15% and 35% in the wells and extracted the related bimolecular recombination coefficient B. By atomistic simulations, they showed that the dependence of B on wavelength is compatible with experimental data and concluded that alloy fluctuations may favor the IQE drop at green wavelengths, which is commonly known as green gap.

Li et al.[67] proposed an alternative method to account for quantum disorder in the classic drift-diffusion model of transport, based on the localization landscape theory.[68] This model gives a good approximation of the density of states of disordered systems, in the range of energies that impact on transport at room temperature. They demonstrated that the landscape maps of electrons and holes can be used to obtain a good estimate of electron and hole overlap and of their impact on IQE. They calculated the integrated recombination current for the uniform QW and the disordered QW model. They demonstrated that for the disordered case, due to the higher (local) carrier density, the integrated Auger recombination can be stronger, compared to a normal QW; they also showed that the different IQE values of the various QWs in a LED can be ascribed to the inhomogeneity of carrier injection.

III. MECHANISMS RESPONSIBLE FOR THERMAL DROOP

This section describes the main processes responsible for thermal droop in LEDs, by presenting a critical review of the most relevant papers in the field. The role of defects, carrier escape, transport processes, and the temperature dependence of the recombination coefficients are described in detail to help the reader understanding the main factors contributing to the thermal droop.

A. Shockley–Read–Hall recombination and thermal droop

1. SRH recombination in LEDs

One of the first reports on the effect of SRH recombination on thermal droop discusses the effect of the indium concentration in the quantum wells.[69] The output optical power of an LED with higher indium molar fraction (25%) was found to decrease more rapidly with temperature compared to a similar LED with only 18% indium. The difference was ascribed to the higher defect density, originated by the higher strain caused by the larger lattice mismatch between the quantum well and quantum barrier layers.

Other than variations in the quantum wells, an additional design parameter that has a significant impact on the thermal droop is the different lattice mismatch with the substrate. By comparing quantum well structures grown on a sapphire or gallium nitride substrate, experimental results show a lower photoluminescence (PL) thermal droop and a longer radiative lifetime for the samples with free standing growth.[70] Both effects are
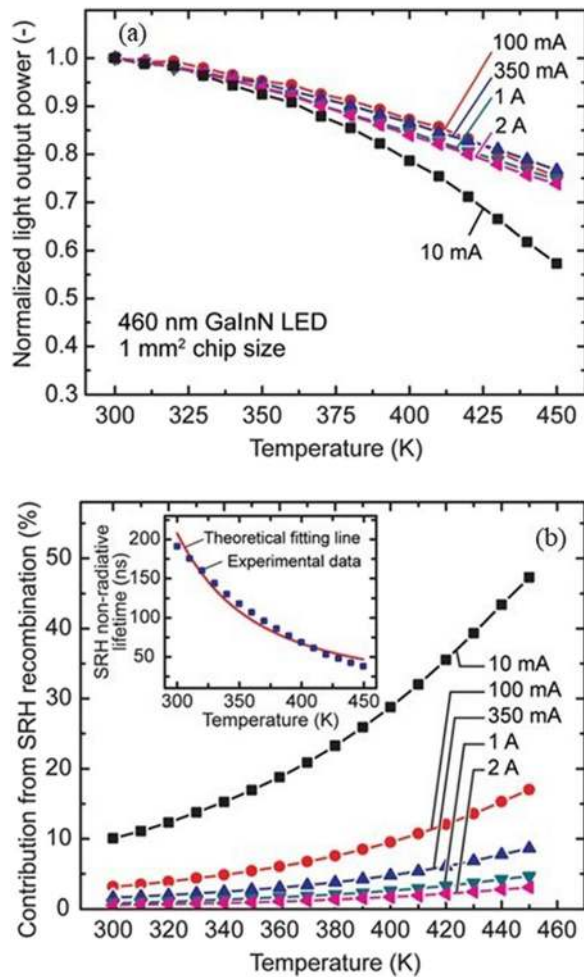
FIG. 7. (a) Normalized light output power as a function of temperature at several operating points. (b) Fraction of SRH non-radiative recombination at different current levels. SRH non-radiative lifetime as a function of temperature and theoretical fit is shown in the inset. Reprinted with permission from Meyaard *et al.*, Appl. Phys. Lett. **99**(4), 041112 (2011). Copyright 2011 AIP Publishing LLC.

at 460 nm. Figure 7(a) shows the measured normalized light output power as a function of temperature at several operating currents.

From the corresponding experimental IQE curves, the excess carrier density in the active region can be approximated as

$$N(I) = \sqrt{\frac{\text{IQE}(I)\,I}{\text{q}BV}}. \qquad (6)$$

SRH recombination is expected to be the dominant loss mechanism at low currents (hence at low N), becoming negligible with respect to Auger recombination and/or electron leakage at high currents (i.e., high N). The fraction of SRH contribution to the total recombination rate is estimated as $\text{SRH}_{\text{ratio}} = AN/R$ and is reported in Fig. 7(b). At low currents ($I \approx 10$ mA), $\text{SRH}_{\text{ratio}}$ exhibits a steep increase with the temperature, raising from 10% at 300 K to more than 47% at 450 K. On the contrary, for $I \approx 2$A, $\text{SRH}_{\text{ratio}}$ does not exceed 4% on the whole considered temperature range. Therefore, the authors conclude that a significant SRH contribution to thermal droop can be observed only at low current.

The same behavior is also reported in Ref. 74, where IQE(I,T) is investigated for several LED diameters. The authors suggested that increasing the diameter is detrimental when high temperature-tolerant LEDs are desired, because of the strong SRH contribution to total recombination at low current densities (5–10 A/cm²).

Reference 75, which compares commercial AlGaInP, InGaN, and AlGaN LEDs, ascribes the temperature dependence of EL in the low-current density regime (0.1 A/cm²) to SRH recombination and hole freeze out. The specific behavior of the quantum efficiency with T depends on the relative strength of these two effects, which is determined by the MQW materials.

Reference 23 does not present a direct study of thermal droop, being focused on the current dependence of the IQE over a broad temperature range for a blue InGaN/GaN MQWs LED. The authors indicate Auger and electron leakage as the dominant mechanisms at high and low temperatures: they also observe that thermal droop is more pronounced at low current densities.

2. SRH recombination in InGaN layers

In order to further describe the effect of Shockley–Read–Hall (SRH) recombination on the temperature-dependent optical performance, we describe here the results of an original experiment. The aim of this activity is to investigate the contribution of SRH recombination in bulk InGaN. To this aim, four set of samples were designed. On a sapphire substrate, a thick unintentionally doped (UID) GaN buffer was grown, followed by a 2.5 μm thick n-GaN layer and by a 0.12 μm thick InGaN layer with varying In molar fraction from 8.5% to 18.5% (see the schematic structure in the inset of Fig. 8). This structure allows for direct photoexcitation of electron–hole pairs in the InGaN layer without any absorption in the upper p-side, which is not present. Moreover, the lack of carrier confinement and the photoexcitation prevent any additional contribution from carrier escape or injection efficiency, leaving non-radiative recombination as the sole possible mechanism responsible for the decrease in the photoluminescence (PL) at higher temperature.

compatible with the reduction in dislocation density throughout the structure due to the variation in lattice mismatch between the substrate and the epitaxial layers.

The effect of the amount of dislocations can be confirmed by testing devices grown on the same substrate but with different threading dislocation densities.[71] The LED with the higher dislocation density has a stronger thermal droop and a smaller non-radiative lifetime, caused by the non-radiative recombination occurring at deep levels associated with dislocations. A similar result, and a reduction in thermal droop by a better AlN nucleation layer, was reported in Ref. 72.

Among the experimental studies identifying SRH recombination as a critical process in thermal droop, Ref. 73 investigated multi-quantum-well (MQWs) LEDs with a photoluminescence peak
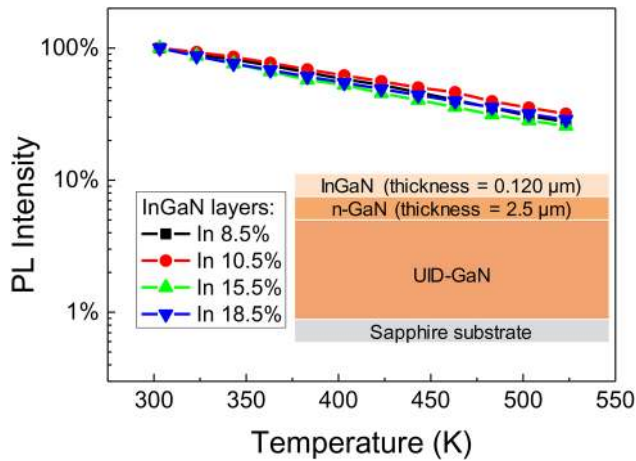
FIG. 8. Thermal droop of the photoluminescence in InGaN layers with different indium content. Inset: structure of the samples under test. Excitation source is a 266 nm pulsed laser, with a repetition rate of 19–20 kHz, pulse width (FWHM) <0.6 nm, average output power >10 mW, and pulse power >7 kW.

FIG. 9. Thermal droop of a representative layer. The experimental data can be reasonably modeled according to the SRH trend predicted by Eqs. (9) and (5). Inset: extrapolated energy position of the deep level responsible for the thermal droop in all the layers under analysis.

Figure 8 reports the variation in photoluminescence for the four layers under test. No anomalous feature can be detected in the temperature range under analysis.

The shape of the PL decrease can be reproduced by the equations modeling the SRH recombination. The photoluminescence intensity is the result of the balance between radiative and non-radiative processes inside the InGaN layer,

$$\text{PL} \propto \frac{Bn}{A + Bn}, \tag{7}$$

where A is the non-radiative recombination coefficient and B is the radiative recombination coefficient in the ABC model (Auger-like recombination processes are neglected here for simplicity).

Given the relations between ABC coefficients and radiative (τ_R) and non-radiative (τ_{SRH}) lifetimes,

$$A = \frac{1}{\tau_{SRH}}, \qquad Bn = \frac{1}{\tau_R}, \tag{8}$$

it is possible to write

$$\text{PL} \propto \frac{\frac{1}{\tau_R}}{\frac{1}{\tau_{SRH}} + \frac{1}{\tau_R}} = \frac{1}{\tau_R} \frac{\tau_R \tau_{SRH}}{\tau_R + \tau_{SRH}} = \frac{\tau_{SRH}}{\tau_R + \tau_{SRH}}. \tag{9}$$

Under the assumption that, for low carrier densities, the SRH recombination lifetime is much lower than the radiative one ($\tau_{SRH} \ll \tau_R$ [76–78]), one can conclude that the PL intensity is directly proportional to τ_{SRH}. According to the SRH recombination theory, under the approximation of near-intrinsic semiconductor and of similar capture rates for electrons and holes, the non-radiative recombination lifetime can be expressed by Eq. (5). Although it is
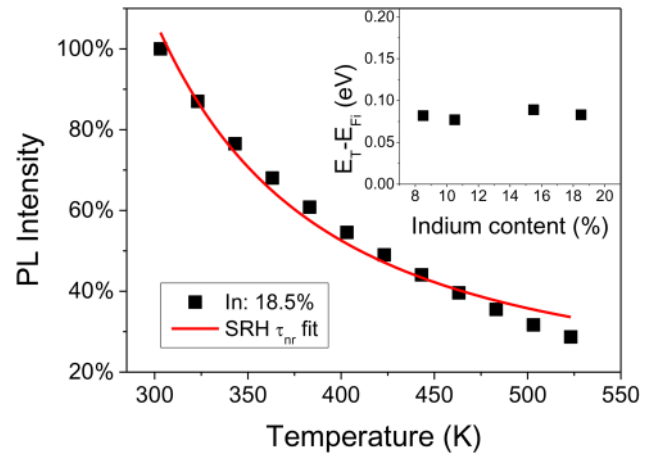
an approximated solution, it was used in the past to model the thermal droop in InGaN LEDs.[73]

Figure 9 reports the good agreement between the experimental data and the fitting by using Eq. (5), confirming that non-radiative recombination through deep levels is the mechanism causing the PL thermal droop. The non-optimal matching may be related to additional effects, such as the temperature dependence of the B coefficient, which will be discussed in Sec. III C. The extrapolated value of $E_T - E_{Fi}$ does not depend on the indium concentration of the layer under analysis (see the inset in Fig. 9), suggesting that the deep level causing the SRH recombination may be the same in every layer. As shown by the experimental data, the defect responsible for SRH recombination is very close to midgap, thus effectively acting as an efficient recombination center.

B. Temperature-dependent capture at defects

In general, in the equations for the SRH recombination in Sec. II B, it is assumed that the capture constants are relatively insensitive to temperature.[38] The SRH equations are not based on any specific capture mechanism but only on the occupation statistics of electrons and holes.[79]

A preliminary remark that applies not only to SRH recombination, but generally to all defect-assisted processes, is that defects induce local deformations in the band structure, possibly leading to potential barriers surrounding the recombination centers. Hence, only carriers with energy exceeding some activation energy can be captured by the deep level, thus undergoing non-radiative recombination.[80]

This capture barrier is created by the local changes in the crystal configuration induced by the lattice defect and by the electron–lattice interaction.[81] Typically, the state of the lattice is represented by a single parameter, called configuration coordinate (Q), which can vary around an equilibrium level. The presence of a trapped charge at a defect state changes the local shape of the
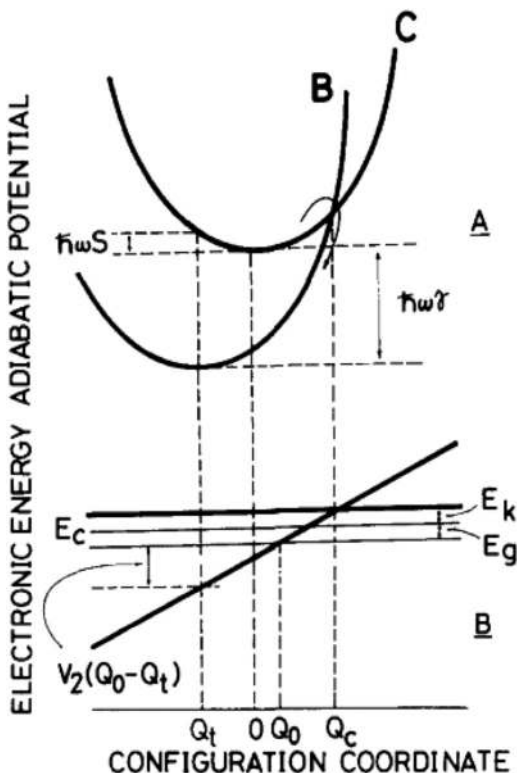
FIG. 10. Configuration coordinate diagram for a generic deep level, showing (a) the full adiabatic potential for the free electron **C** and trapped electron **B**, and (b) the electronic energy. Reprinted with permission from Goto *et al.*, J. Appl. Phys. **54**(4), 1909–1923 (1983). Copyright 1983 AIP Publishing LLC.

FIG. 11. (a) Sketch of the potential profile close to a deep level and (b) improved approximation based on an inverted Morse potential. Reprinted with permission from Goto *et al.*, J. Appl. Phys. **54**(4), 1909–1923 (1983). Copyright 1983 AIP Publishing LLC; and Buchwald and Johnson, J. Appl. Phys. **64**(2), 958–961 (1988). Copyright 1988 AIP Publishing LLC.

lattice, leading to a new value of the configuration coordinate and to a different lattice equilibrium state. The adiabatic potential in the two cases is shown in Fig. 10(a), where **C** is the "free" Bloch electron state and **B** is the trapped electron. Since the transition between the free and the trapped state can only happen when the adiabatic potential is conserved (i.e., at the crossing point from the **C** to the **B** state), it is possible to notice that the free electron, located at the potential minimum of state **C**, has to overcome a small potential barrier in order to enter the deep level. After the crossing point, the electron relaxes down to the minimum of state **B**, losing energy by phonon emission. For this reason, this process is called capture by multiphonon emission (MPE). As the electron relaxes to the new energy minimum, the lattice itself relaxes to a new spatial configuration, explaining why the two adiabatic potential minima are located at different values of the configuration coordinate. A detailed analysis of the electron–lattice interactions including several second-order effects can be found in Ref. 82.

The physical origin of the capture barrier is twofold, as summarized in Fig. 11(a).[83] The defect itself, depending on its charge state, generates a short-range potential variation, which can be approximated as a potential well with depth V_0, corresponding to the thermal activation energy for the emission from the deep level E_a, and size

limited by the distance a with the nearest neighbors (in the neutral charge state). Moreover, the presence of the defect breaks the periodicity of the lattice, leading neighboring nuclei to shift their equilibrium position, a variation that causes a variation in the potential for electrons. The amplitude of this variation is proportional to the lattice displacement $Q - Q_0$ (with proportionality constant V_1) and influences the potential up to a distance b. The total potential profile is the superposition between the two effects, shown in Fig. 11(a), causing the presence of a potential barrier for an electron located at $r > b$ to be trapped at $r < a$. The accuracy of the simple sketch of the potential profile can be improved by considering more accurate

potential models, such as the inverted Morse potential reported in Ref. 84, which leads to the final potential profile close to the deep level reported in Fig. 11(b).

The presence of defect capture barriers as sources of thermal droop is reported for the gallium arsenide material system, possibly related to nitrogen impurities[85] and for the gallium phosphide.[86] In the gallium nitride material system, relatively large values of confining potentials originating the thermal droop, not compatible with composition fluctuations, have been attributed to non-radiative recombination centers with capture barriers.[87]

C. Dependence on temperature of recombination coefficients

The dependence of the recombination coefficients on temperature can also play a role in the thermal droop.

The A coefficient shows a very simple temperature dependence; it increases as theoretically predicted by Eqs. (3) and (5).

The analysis of the radiative recombination coefficient is more complex. Theoretically, in a bulk material, the bimolecular coefficient can be expressed as[88]

$$B = \frac{1}{\tau_R N_C} \left(\frac{m_r}{m_v} \right)^{3/2} \qquad (10)$$

where m_r is the reduced effective mass, m_v is the effective mass for the valence band density of states, and N_C is the effective density of states in the conduction band,

$$N_C = \frac{1}{4} \left(\frac{2 m_c^{\star} k_B T}{\pi \hbar^2} \right)^{3/2}, \qquad (11)$$

with $m_c^{\star}$ being average effective mass of the conduction band. Therefore, not considering the variation in τ_R, the final temperature dependence is $B(T) = B_0 T^{-3/2}$. If a quantum well is taken into account, the carrier confinement and quantization of the energy level leads to the temperature dependence $B(T) = B_1 L T^{-1}$.[89]

These simple theoretical expectations are not always accurate, and more advanced fully microscopic models can be used to predict the temperature dependence of the radiative current.[54] In the case of InGaAsP structures, results show that it varies significantly depending on the carrier density, ranging from a $\propto T^{-3}$ trend at low density to a $\propto T^{-1/2}$ approximation at high density up to 250 K, whereas the dependence becomes stronger and exceeds $\propto T^{-1}$ for the highest temperatures. The discrepancy with respect to the theoretical calculations is ascribed to the limited validity of the Maxwell–Boltzmann approximation at high carrier density and phase-space filling. In an additional work, the same authors modeled the experimental data obtained on InGaN LEDs with different emission wavelength with a density-activated defect recombination (DADR) mechanism, finding a $\propto T^{-7/4}$ dependence.[90] Recent studies on high-quality InGaN single-quantum-well LEDs suggest that, at low current, the B coefficient decreases with temperature due to the Coulomb interaction between electrons and holes; at high current, B can increase due to the screening of the internal field, which increases the electron–hole wavefunction overlap.[25]

A simple analytical expression for the temperature dependence of the Auger coefficient has been proposed in Refs. 54 and 91, assuming a parabolic band structure and Boltzmann statistics,

$$C(T) = C_0 \exp \left(-\frac{E_a}{k_B T} \right), \qquad (12)$$

where C_0 is the Auger coefficient at room temperature and E_a is the activation energy. The exponential temperature dependence in (12) is typical of direct (i.e., band-to-band) Auger processes with an activation energy. The Auger threshold in InGaN alloys with In contents of interest for blue LEDs is too large to allow significant direct Auger processes. On the other hand, as specified above, indirect transitions (i.e., assisted by phonons, impurities, or defects) are possible below threshold, as the excess momentum/energy is provided by the additional particle. Indirect processes are of second order in perturbation theory, which means that their transition probability should be smaller; nevertheless, they may compete with direct processes as the number of possible final states increases. Being threshold-less, indirect Auger coefficients depend weakly on temperature,[92] suggesting that the activation energy E_a in (12) would be smaller than typical values obtained for the band-to-band process. More often, the temperature dependence of C is modeled with a power-law function of temperature.[93,94] All bulk calculations of indirect Auger rates are monotonically increasing with temperature,[57,94,95] as expected from phonon occupation numbers and carrier statistics. Other effects such as the temperature dependence of the band structure may play a secondary role. Moreover, phonon-emission-assisted Auger recombination is expected to contribute even at absolute zero temperature because of phonon spontaneous emission originating from zero-point fluctuations of the vibrational field.[96] This could explain experimental results for droop at very low temperatures.[97]

Auger rates may be significantly enhanced in confined nanostructures with respect to the bulk case, since conservation of momentum is lifted in the direction(s) in which the periodicity of the crystal is broken, leading to the appearance of direct threshold-less recombination channels.[98] Therefore, for narrow quantum wells, we may expect the 2D Auger coefficient (cm^4/s) multiplied by W^2 to exceed the 3D coefficient of the bulk material (cm^6/s), owing to the predominance of the (quasi-)threshold-less processes and a smooth transition to the bulk case as W is increased. [Note: The distinction between 3D and 2D Auger coefficients is somewhat hazy, at least in a wide bandgap context, in the same way as it is arbitrary to distinguish between localized and delocalized carrier populations in a quantum-corrected semiclassical approach to carrier transport. More to the point, even if we may assume that the initiating carriers populate localized states of the nanostructure, the rebound electron (the one that takes the excess energy) will be promoted to a delocalized state far away from the conduction band edge, calling for a unified description of localized and extended states within a full-Brillouin-zone framework.] Here W is the thickness of the confinement region (typically the thickness of the quantum well). Such direct threshold-less transitions have a weak non-exponential temperature dependence similar to that of indirect

processes. In general, C is not anymore a material property but has to be evaluated microscopically for the nanostructure of interest, the result depending, e.g., on well width, bias, carrier confinement, and polarization field. The complexity of this point is exemplified by the difference between the microscopic calculations of the effects of the confinement potential profile on Auger rates performed by Vaxenburg et al.,[99,100] which predict smaller C's with graded quantum-well interfaces, and by Hader et al.,[65] where the use of a less simplified Auger model leads to almost negligible differences between ideal abrupt interfaces and gradual barrier–well transitions. Due to the interplay between the momentum transferred in the Coulomb interaction (dictated by temperature) and the Coulomb matrix element involved in direct threshold-less transitions, C is not necessarily a monotonic increasing function of temperature.[92] An "anomalous" temperature behavior of C has been observed indeed for blue high-brightness InGaN/GaN LEDs[22] and InGaN quantum-dot laser diodes emitting at 630 nm.[101] Another possible reason for the decrease of C with temperature is the thermal spill-over of carriers into bands where Auger transitions are forbidden or reduced by selection rules.[54] The temperature dependence of C is also deeply connected to its carrier density dependence. For example, the relative importance of thermal carrier spill-over is weakened for increasing carrier density, so that the decoupling of temperature and density dependencies is not possible in general.[54]

The "apparent" behavior of C vs temperature, as extracted from experiments/calculations, ultimately depends on which mechanism dominates. This conclusion is supported by a recent body of experimental studies identifying TAAR as a significant loss process in high-defect-density LEDs.[17,58] Also, thermal droop appears to be affected by TAAR in conventional devices,[102] while low-defect-density LEDs grown on GaN substrates, where TAAR is expected to be negligible, show nearly temperature-independent recombination rates,[3,25] suggesting that thermal droop there is determined by transport effects (see Fig. 12 for a representative schematic of the TAAR process).

D. Impact of carrier transport, escape, and freeze out on thermal droop

In addition to the non-radiative recombination processes discussed above, several transport-related processes may favor thermal droop, including carrier escape (i.e., the thermionic escape of carriers from the wells), carrier overflow (related to the position of the Fermi level with respect to the quantum barrier), or tunneling through the barriers. Recent studies (see, for instance, Ref. 25 pointed out the important role of transport processes in the thermal droop. In this section, we consider the impact of transport-related phenomena by focusing on carrier escape, localization effects, the characterization of carrier leakage from electroluminescence (EL), the hole freeze out and its effect on external quantum efficiency, and consideration on the interpretation of Stokes shift in InGaN quantum wells.

Since carrier transport results from the superposition of several effects, it is hard to identify clear signatures of its impact on the IQE at standard temperature and injection conditions. This is why many of the investigations described in the literature are performed on extended temperature and/or injection ranges, with the aim of exacerbating only one or few of the phenomena. This allows us to deepen the understanding of the physics in the devices, with the theoretical support of analytical,[103,104] rate equation,[105–108] or semiclassical[14] models. In III-nitride materials, identifying models and experiments is particularly challenging due to peculiar features not present in most "conventional" semiconductors, e.g., a strong asymmetry between the acceptor and donor doping ionization energies, and the presence of strong polarization fields. These peculiarities act as wild-card factors in III-nitride devices, since the effect of both carrier asymmetries and polarization fields influence several aspects of carrier transport and make thermal droop an even more intricate tangle.

The sensitive point of experiment-driven modeling is "fitting." However, this may be considered a simplified approach, since it demonstrates an unawareness of the "exact" transport and recombination properties in nanostructured materials. In this view, moving from semiclassical (although possibly "quantum-corrected"[109]) to quantum kinetic approaches such as the non-equilibrium Green's
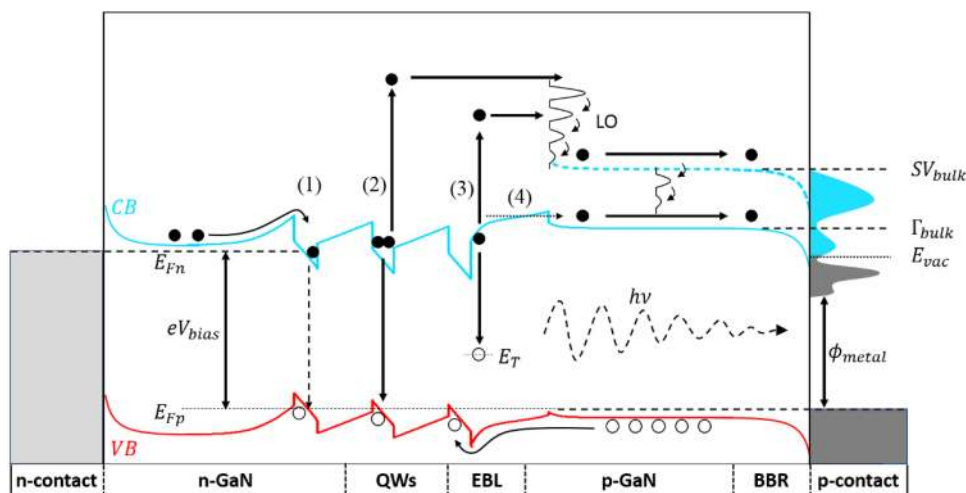

FIG. 12. Relevant electron energy levels, transport, recombination mechanisms, and the corresponding electron emission spectrum. (1) Radiative recombination, (2) interband Auger recombination, (3) TAAR in EBL, and (4) thermal escape. Reprinted with permission from Myers et al., Phys. Rev. B **100**, 125303 (2019). Copyright 2019 American Physical Society.

function (NEGF) theory could provide more realistic descriptions of the optical and electronic interactions without resorting to pseudoempirical fitting parameters.[110]

A general effect is always associated with a higher temperature: a corresponding increase in energy of the body whose temperature rises. Electrons and holes in semiconductors are also affected by this process, causing possible additional thermal droop in every device where a potential barrier is present. We can differentiate them in two main classes. If the thermal energy gained by the carrier is small, the carrier can move outside shallow potential minima present inside the quantum well, breaking the exciton before it can recombine radiatively. This effect is known as exciton delocalization. However, if the carrier energy increase is high, it can be enough to overcome the confining potential barrier in the quantum well, entirely removing the electron or hole from the quantum well. In this second case, the process is referred to as carrier escape from the quantum wells. In the following, we will analyze both processes in detail.

1. Exciton delocalization

The first step to prove the effect of exciton delocalization is to demonstrate the presence of potential fluctuation in the structures under test. This can be done by the observation of Stokes-like shift and by the presence of a large FWHM of the free excitonic (FE) resonance.[111] The potential fluctuations can be the result of various lattice configurations, originated by different growth parameters and conditions, and therefore lead to a different macroscopic behavior, summarized in Fig. 13.[111]

The first possible origin, monoatomic fluctuations in the quantum well thickness, causes different values of the lowest allowed energy level in specific spatial locations, without any change in energy gap value. They lead excitons to localize in the thicker positions, where the ground state is at lower energy. The sharp potential edges produce a QW-like behavior, but the relatively weak potential fluctuation is associated with a small potential barrier.
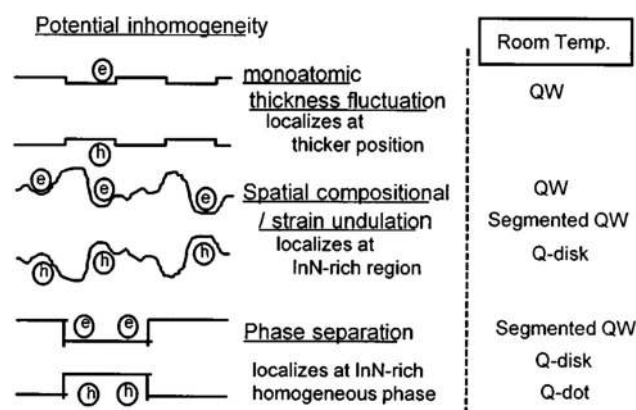

FIG. 13. Summary of the possible causes for exciton localization, including their effect, schematic band diagram, and equivalent behavior. Reprinted with permission from Chichibu, J. Vac. Sci. Technol. B **16**(4), 2204 (1998). Copyright 1998 AIP Publishing LLC.

A second possible origin is spatial compositional variations or strain undulation, which cause local variations in the energy gap value. Therefore, the exciton will localize in the regions where the energy gap is the lowest, i.e., in correspondence of the low-gap material rich regions (indium in the case of the gallium nitride material system). In this case, the potential fluctuations are still weak, since the local compositional or strain variation cannot be present in high magnitude; in addition, the potential profile is not sharp, due to the continuous (and not discrete) variation in In composition. This leads to a macroscopic behavior as quantum well, segmented quantum well, or quantum disk, depending on the lateral size.

The third situation is the complete phase separation during growth, which creates wide regions with lower energy gap where excitons can localize, such as InN-rich homogeneous phase in GaN. The complete phase separation creates large and sharp potential barriers, and these regions can behave as segmented quantum wells, quantum disks, or quantum dots depending on their size.

Experimentally, the exciton delocalization causes a significant thermal droop, visible at cryogenic temperature due to the small barrier height, which increases at higher indium content.[112] This effect can be detected also in other material systems.[85,113] The amount of thermal droop related to exciton delocalization decreases in magnitude at high excitation or injection intensities, since higher exciton densities in the quantum wells can fill both the low- and high-potential fluctuation regions, effectively limiting the delocalization process.[104]

Carrier localization processes have been indicated to play a relevant role in the thermal droop in early literature on the topic, from the late 1990s and the early 2000s. Typically, localization of excitons at potential fluctuations may impact on the IQE of LEDs already at low temperatures. In 1998, Leroux et al.[114] demonstrated that excitons are localized at low temperature: they showed that the luminescence at 9 K originates from localized excitons, with binding energy of the order of 20 meV, in the case of wide wells, and 46 meV, in the case of five-monolayer wells. In addition, they showed that when temperature is increased, the QW PL energy first increases (for low temperatures, below 100 K) and then decreases (for higher temperatures). They ascribed this effect to the delocalization of QW excitons, induced by temperature.

A further contribution on the topic was presented by Cho et al.:[115] they studied both the changes in PL energy and the variations in PL intensity as a function of temperature. They proposed that the thermal emission of carriers out of potential minima toward high energy states located in the wells is the dominant mechanism responsible for the thermal quenching in InGaN photoluminescence. They suggested that alloy fluctuations and/or interface roughness in the quantum wells can significantly impact on localization effects.

Grandjean et al.[26] investigated the role of localization processes and non-radiative effects related to threading dislocations in UV samples grown on sapphire and on GaN substrates. The samples were grown by molecular beam epitaxy (MBE) and differ in the dislocation density: $5 \cdot 10^9 \, \mathrm{cm}^{-2}$ for the one grown on sapphire and $<10^5 \, \mathrm{cm}^{-2}$ for the homoepitaxial one. They showed that the spectral features at 10 K are similar for the two samples, except the integrated PL intensity, which for the homoepitaxial sample is twice that of the heteroepitaxial one. Such a difference was found to be

much stronger at room temperature, with the PL of the homoepitaxial sample being 20 times higher than the other. The authors argued that the higher luminescence of the homoepitaxial sample cannot be explained by a better confinement, since the two structures are the same, apart from the substrate and dislocation density. Another factor that may—in principle—explain the different behavior of the two samples is a different carrier localization. They estimated the degree of exciton localization from the variation of PL energy as a function of temperature. They demonstrated that the localization energy is rather low (18 meV) and equivalent for the sample grown on sapphire and the one grown on GaN. So, the higher efficiency at room temperature of the sample grown on GaN could not be explained by a stronger carrier localization. The authors then studied the role of threading dislocations on the thermal droop, by analyzing the temperature-dependent PL intensity. They used an Arrhenius analysis, under the hypothesis that in steady-state, the PL intensity depends on the temperature according to

$$I = \frac{I_0}{1 + A \exp\left(-\dfrac{E_a}{k_B T}\right)}, \tag{13}$$

where E_a is the activation energy of the non-radiative process responsible for thermal droop. Grandjean et al.[26] demonstrated that this equation can reproduce well the experimental data obtained on the LED grown on the GaN substrate. They found an activation energy equal to 125 meV, which is consistent with the energy distance between the well and the barrier. Thus, they concluded that the drop in luminescence above 100 K can be ascribed to the thermal escape of carriers from the well to the barriers.

On the contrary, they found that the PL signal of the LED grown on sapphire (with high dislocation density) decreased at low temperature, and they ascribed this effect to the non-radiative recombination of excitons at dislocations. With increasing temperature, the population of free excitons is supposed to increase, due to the low localization energy (18 meV). This results in a decrease in the PL signal: free excitons can move along the xy QW plane, thus easily reaching dislocations. In a highly defective material, Eq. (13) does not reproduce correctly the experimental data; one has to include the non-radiative losses as follows:

$$I = \frac{I_0}{1 + A_1 \exp\left(-\dfrac{E_{a1}}{k_B T}\right) + A_2 \exp\left(-\dfrac{E_{a2}}{k_B T}\right)}. \tag{14}$$

Through fitting of the experimental data, they found $E_{a1} = 125$ meV (consistent with carrier escape, as explained above) and $E_{a2} = 12$ meV (accounting for the detrapping of excitons from potential fluctuations). Similar numbers were given also by Rossi et al.,[116] who reported a comparison between electroluminescence and cathodoluminescence.

Cao et al.[117] investigated MQW LEDs and considered samples with identical structures but varying indium content in the wells. They did a rate equation analysis and indicated that the density of localized states in green LEDs is two orders of magnitude higher than in UV LEDs. They indicated that, for green LEDs, radiative recombination at localized states is the dominant emission process

in the whole analyzed temperature range. On the contrary, for UV LEDs, this process dominates only at low temperatures.

In a later report, Wu et al.[118] proposed to use Si delta doping to improve the quantum efficiency and thermal stability of MQW LED structures. Through this approach, they demonstrated an increase in the activation energy from 115 meV to 140 meV. They ascribed this improvement to the supply of electrons from the delta doping barrier region, and to the increase in the capture of holes, by the higher barrier in the valence band. They suggested that Si delta doping can strongly reduce carrier leakage, thus improving the quantum efficiency of the devices.

The role of localization effects was analyzed also by Jiang et al.,[119] who investigated the efficiency droop behavior of green InGaN LEDs as a function of temperature, between 300 K and 480 K. They showed that around the onset of the efficiency droop, the EL peak shows a monotonic blueshift, and a reduction of the full-width at half maximum (FWHM), with increasing current. They ascribed this effect to the filling of localized states within the MQWs. On the other hand, with increasing temperature, they detected a redshift of emission, ascribed to bandgap narrowing. However, they demonstrated that from 300 K to 480 K, the peak energy shift is 17 meV, which is much lower than what expected from the Varshni formula (35 meV); according to the authors, this result further confirmed the presence of thermally enhanced carrier delocalization. Carrier localization could also explain the reduction of FWHM at high current levels; in fact, localized states typically have a band tail like distribution, and the states with higher energy have a high density of states.[119]

A different approach was used by Mickevičius et al.,[120] who analyzed the temperature-dependent optical characteristics of AlGaN epitaxial layers and quantum wells. They suggested that the loss in efficiency at high current density is influenced by the carrier thermalization conditions and the ratio between carrier thermal energy and localization depth. Specifically, they evaluated the impact of the ratio $k_B T/\sigma$, where σ is the localization parameter,
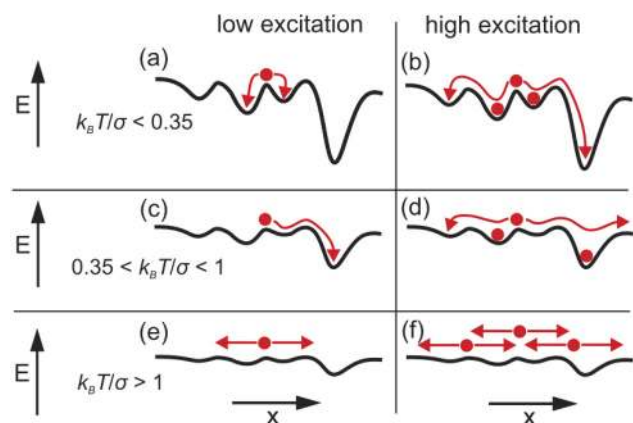

FIG. 14. Schematic diagrams of carrier transport at low [(a), (c), and (e)] and high [(b), (d), and (f)] excitation. Reprinted from Mickevičius et al., AIP Adv. **6**, 045212 (2016). Copyright 2016 Author(s), licensed under a Creative Commons Attribution (CC BY) license.

describing the dispersion of the depth of potential fluctuations (see also Fig. 14 for details). They demonstrated that for non-thermalized carriers (having $k_B T/\sigma < 0.35$), droop occurs due to the redistribution of non-thermalized carriers. At higher temperatures ($0.35 < k_B T/\sigma < 1$), droop originates from the increased non-radiative recombination: localized states are filled, and more and more carriers become de-localized. In the presence of high temperatures or weak localization ($k_B T/\sigma > 1$), other processes as stimulated emission or transport to extended defects may also play a role.

2. Carrier escape from the quantum wells

The potential barrier height for emission of carriers from the quantum wells to the quantum barriers is significantly higher than the one for exciton delocalization; therefore, carrier escape from the quantum wells can usually be noticed at room temperature and above, rather than at cryogenic temperatures. Escape processes are particularly strong for all the material systems used for long-wavelength emission in the red and infrared spectral range, where the quantum barrier is lower due to the narrower energy gap of the involved materials.

In the gallium arsenide material system, the thermal droop caused by thermionic emission from the quantum wells can still be detected at cryogenic temperature and can be proved by comparing the extrapolated values of the activation energy with the theoretical barrier heights in devices with different quantum well thickness.[121] By adding aluminum in the quantum barriers to increase the barrier height, it was possible to eliminate the thermal droop caused by carrier escape, creating an additional thermal droop process tentatively ascribed to SRH recombination.

The presence of a barrier height-related thermal droop was reported also for the gallium nitride material system, showing an improvement in the thermal stability of the electroluminescence when the indium content in the quantum wells is increased from 5% to 18%.[69] A possible contribution from the internal electric field to the thermionic emission is suggested sometimes.[108,122]

Additional information on the carrier escape is present in Ref. 73, which was previously analyzed with reference to the low-bias region in Sec. III A 1. At high current levels, the optical power decrease with the temperature is found to be stronger than at intermediate current levels. The authors model the decrease with an additional recombination term in the ABC model, which contains dependence on second, third, and higher order terms of n. This term is ascribed to electron leakage from the active region, including electrons not being captured by the quantum well, more electrons available for overflow due to the lower radiative efficiency, higher level of thermionic field-assisted emission, or defect-assisted tunneling through the electron blocking layer.

Temperature- and current-resolved electroluminescence (EL) spectral intensities present several features that can help acquiring deeper understanding of the causes of thermal droop. Examples of EL investigations are reported in Refs. 105–107, which present a comparative study of the spectra of superbright InGaN single-quantum-well (SQW) LEDs emitting in the green (45% In molar fraction) and blue (20% In molar fraction) ranges.[123] In Fig. 15, the wavelength-integrated EL intensity of
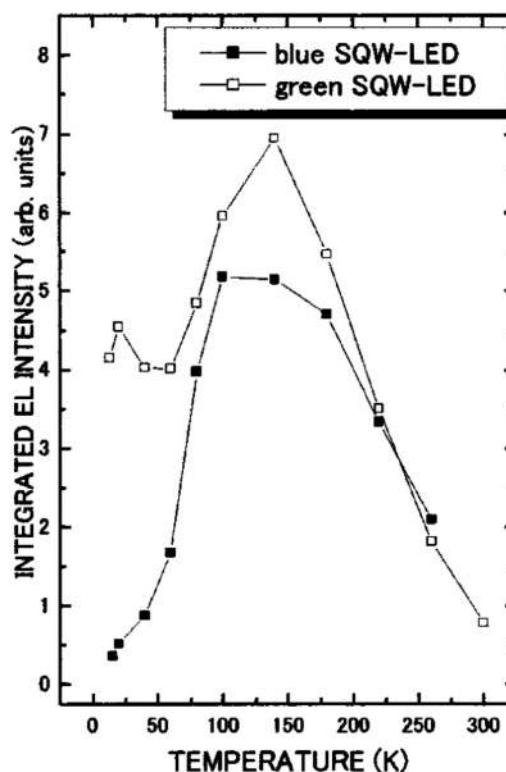

FIG. 15. Wavelength-integrated EL intensity of the green and blue SQW LEDs as a function of temperature. Injection current level used for this plot is 0.1 mA. Reprinted with permission from Hori *et al.*, Appl. Phys. Lett. **79**(22), 3723–3725 (2001). Copyright 2001 AIP Publishing LLC.

two green and blue LEDs are reported vs the temperature for 0.1 mA injection current.

It can be noted that the EL reduction at low temperatures is quite strong especially for the blue diode. To study this phenomenon in further detail, Fig. 16 shows the EL spectral line shapes as a function of injection current for the green (a) and blue (b) LEDs. In the range of 140–300 K, where the EL efficiency is high, the spectral line shape changes with current, and the contributions from the transitions between localized states with higher energies can be noticed. This demonstrates that, in this temperature range, electrons and holes are captured effectively by the SQW. On the other hand, at cryogenic temperatures (20 K), the line shape reported in Fig. 16(a) is just mildly current-dependent, suggesting that no band filling takes place due to poor carrier capture in the green LED. This is even more pronounced for the blue LED, as shown in Fig. 16(b), where inefficient carrier capture leads to strong electron leakage, as one can notice from the 3.1 eV emission peak, clearly related to emission from GaN barriers.

A common remedy for electron leakage is the introduction of AlGaN electron blocking layers (EBLs)[14] preventing the electrons from escaping toward the *p*-doped region. However, EBLs are not a
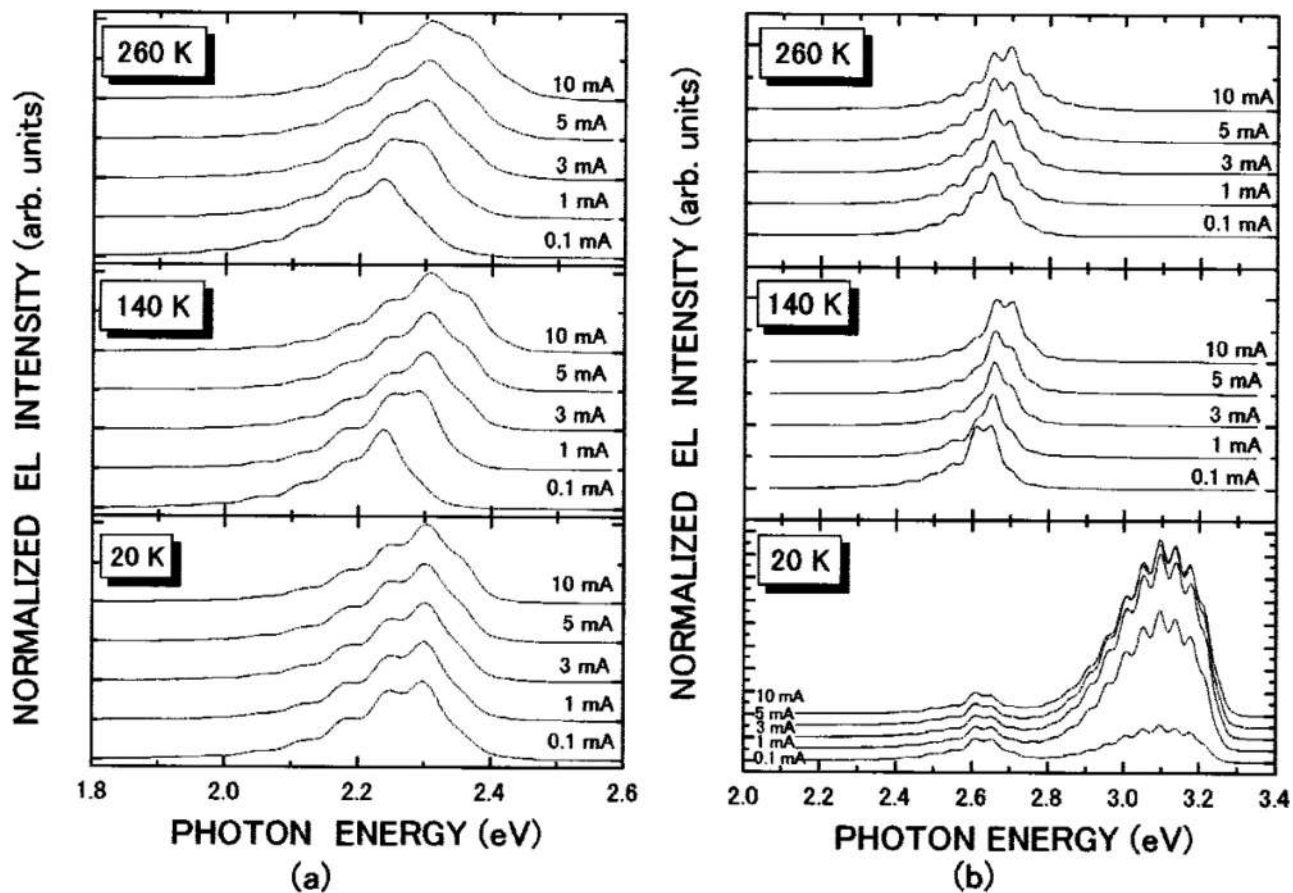
FIG. 16. EL line shape variations of (a) green and (b) blue InGaN SQW LEDs as a function of injection current at 20, 140, and 260 K. The intensity is normalized to the highest SQW peak in each spectra. The baselines are vertically shifted for a clear comparison. Reprinted with permission from Hori *et al.*, J. Appl. Phys. **93**(6), 3152–3157 (2003). Copyright 2003 AIP Publishing LLC.

perfect solution. In fact, they behave as potential barriers also for the holes moving from the *p*-doped section toward the active region. Moreover, EBLs do not contrast (and instead are affected by) polarization effects. In fact, due to the comparative lack of symmetry of the hexagonal crystal structure, III-nitride materials exhibit polarization features even for strain-free heterostructures, which are referred to as "spontaneous polarization" and can be quantified as a function of the In molar fraction x as

$$P_{SP} = (1 - x)P_{SP,GaN} + xP_{SP,InN}, \qquad (15)$$

where the values of the GaN and InN spontaneous polarization $P_{SP,GaN}$ and $P_{SP,InN}$ can be found in Ref. 124. In addition to spontaneous polarization, a piezoelectric component is induced by the lattice mismatch between layers with different compositions,[51,125]

$$P_{PZ} = 2\frac{a - a_0}{a_0}\left(e_{31} - e_{33}\frac{c_{13}}{c_{33}}\right), \qquad (16)$$

where a_0 is the lattice constant of the material layer, a is the lattice constant of the buffer layer or substrate, e_{31} and e_{33} are elements of the piezoelectric strain tensor, and c_{13}, c_{13} are the elastic constants of the material under consideration. The model parameters can be determined by linear interpolation [as in (15)] between the GaN and InN values provided in Ref. 124. The effect of polarization is introduced in the electrostatic model of the device by considering terms of fixed sheet charges ρ_p located at the heterointerfaces computed as[126]

$$\rho_p = -\nabla P = -\nabla\left[P_{SP} + P_{PZ}\right]. \qquad (17)$$

The Coulomb field combines with the polarization field, enhancing electron tunneling into the *p*-type region and leading to an increased leakage current.[108] In this view, polarization engineering is essential to mitigate the efficiency droop through an improvement of the electron and hole carrier transport features.[14,23,127,128]

3. Hole freeze out and external quantum efficiency

Carrier freeze out, usually observed in conventional semiconductors at cryogenic temperatures when the thermal energy cannot ionize all the dopants, is relevant also at room temperature in p-type III-nitrides, as in most wide-bandgap material systems, due to the high ionization energies of the acceptors. In particular, GaN exhibits a large ionization energy of the acceptors ($\Delta E_A \sim 170$ meV) compared to the donors ($\Delta E_D \sim 15$ meV), leading to asymmetric carrier transport and poor hole injection.[75] The steady-state density of ionized acceptors can be written as (last expression is exact in the nondegenerate limit),[129,130]

$$N_A^- = \frac{N_A}{1 + g_A \exp\left(\dfrac{E_A - E_F}{k_B T}\right)} \sim = \frac{N_A}{1 + g_A \dfrac{p}{N_V} \exp\left(\dfrac{\Delta E_A}{k_B T}\right)}, \quad (18)$$

where p is the hole density, g_A is the degeneracy factor (equal to 4 in III-nitrides), N_V is the effective valence band density of states, and the ionization energy ΔE_A is defined as the distance of the impurity energy level from the valence band edge.

Figure 17 illustrates the impact of partial hole freeze out comparing the temperature-dependent EQE characteristics (reported in arbitrary units, A.U.) of three devices characterized at 0.1 A/cm^2 injection: a red AlGaInP LED, a blue InGaN LED, and a deep ultraviolet (DUV) AlGaN LED.

The AlGaInP red LED and the InGaN blue LED show similar tendencies, i.e., an increasing EQE with decreasing temperature. It can be noticed that the EQE(T) variation is more markedly pronounced for the red LED, for which it also exhibits a trend acceleration below 190 K. Instead, the AlGaN DUV led shows an opposite trend, since the EQE decreases with decreasing temperature, with a trend acceleration below 180 K. The argument behind the discussion proposed in Ref. 75 is based on the asymmetry between donor and acceptor concentrations, which are quite similar for AlGaInP (so that SRH is the main limiting factor of the EQE), more unbalanced in InGaN, and very different in AlGaN. This argument is supported by the study reported in Fig. 18, which compares the impact of SRH recombination and acceptor dopants activation on the EQE.

4. Interpretation of Stokes shift in InGaN quantum wells

Several experimental studies on InGaN quantum wells report of the presence of a non-zero energy difference between the photocurrent (PC, or "absorption") and electroluminescence (EL, or "emission") spectra, commonly referred to as Stokes shift.[105,107,111] In "traditional" materials, the Stokes shift is a signature of inhomogeneity of the potential, which is reflected in the effective bandgap. This could be ascribed to the phase-separating nature of InGaN, to the fluctuation of monolayer thicknesses, and/or to spatial compositional (or strain) undulations. In these situations, electron–hole pairs localize in potential minima, giving rise to free excitonic (FE) resonances.[111,131,132]

As an example, here the photocurrent and electroluminescence spectra are reported from Fig. 19 for the blue and green InGaN LEDs at 15 K and 260 K.
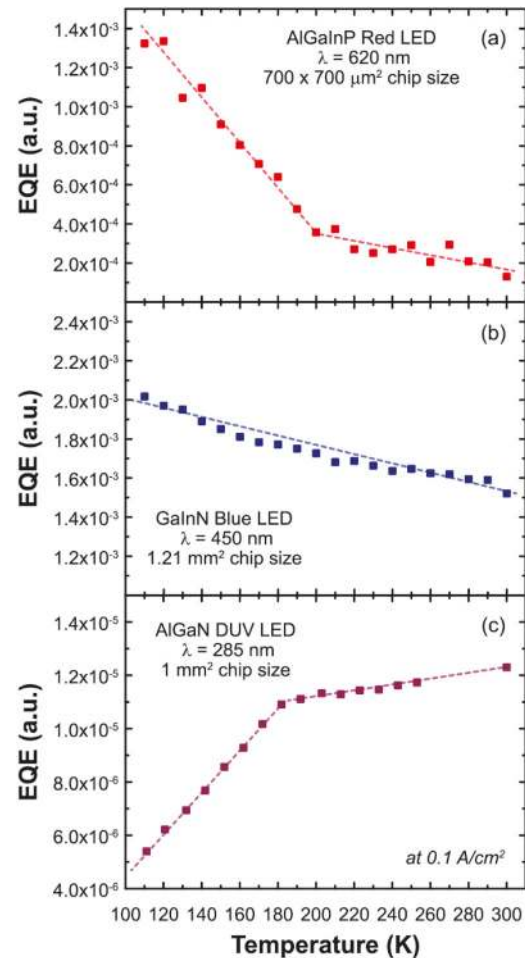

FIG. 17. Temperature-dependent EQE curves for (a) AlGaInP red LED, (b) GaInN/GaN blue LED, and (c) AlGaN DUV LED measured at 0.1 A/cm^2. Reprinted with permission from Park *et al.*, J. Appl. Phys. **119**(2), 023101 (2016). Copyright 2016 AIP Publishing LLC.

In III-nitride nanostructures, Stokes shifts can be hardly ascribed just to excitonic effects. Indeed, very high quality InGaN/GaN QWs demonstrate Stokes shifts as large as 60 meV,[133] even though calculations based on the measured potential fluctuations predict values around 14 meV.[134]

This difference could be related to the quantum-confined Stark effect (QCSE) in the presence of multiple localized states. In a symmetric QW in flatband conditions (no electric field, no QCSE), this could not take place. In fact, the states with odd and even quantum numbers are symmetric and antisymmetric, respectively. Therefore, in this setting, only the transitions between states with the same parity are allowed. On the other hand, in the presence of QCSE, even and odd states mix, at the point that the transition forbidden in the no-field case becomes dominant, as sketched in Fig. 20. In this situation, absorption is likely to take place at an
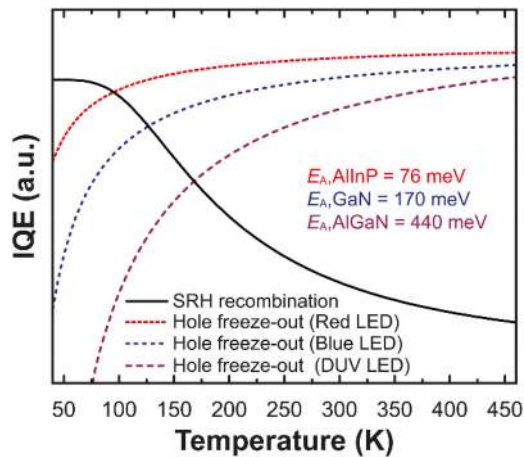
FIG. 18. Calculated factors influencing the temperature dependence of the EQE curves, including SRH recombination (solid line) and hole freeze out effects in AlGaInP red LED, GaInN blue LED, and AlGaN DUV LED (dashed lines). Reprinted with permission from Park *et al.*, J. Appl. Phys. **119**(2), 023101 (2016). Copyright 2016 AIP Publishing LLC.

excited state (increasing the corresponding peak energy), and the ground states are pushed toward the walls of the QW (leading to a decrease of their transition energy and therefore red-shifting the emission spectrum peak).

By completing the theory based on potential fluctuations with the aforementioned QCSE description, good predictions of the Stokes shift

can be achieved at temperatures greater than 120 K.[133] At cryogenic temperatures, this description can be further improved by including the effect of carrier freeze out, which leads to an additional shift.

E. Non-SRH defect-related processes

The impact defects can have on the optoelectronic properties and on the thermal droop is not limited to their role in SRH recombination, already discussed in Sec. III A. Shallow states, such as the ones introduced by the doping of the semiconductor, can have a significant impact on the temperature-dependent luminescence, visible at low temperature, due to processes that differ from the non-radiative recombination through deep levels. Moreover, the presence of deep levels can contribute to the thermal droop even when they are not located in the layer where the band-to-band recombination is occurring, by assisting the carrier escape process.

1. Thermal droop in doped semiconductors

The analysis of the thermal droop on doped semiconductors may seem irrelevant, since the quantum wells are never intentionally doped. However, its significance increases if the diffusion of dopant and contaminants inside the quantum well during operation is taken into account, such as magnesium and hydrogen in gallium nitride[135–138] or zinc and carbon in indium phosphide.

A detailed and comprehensive analysis of the doping effect on thermal droop was carried out in Ref. 140, by testing temperature-dependent photoluminescence in undoped, *n*-doped (Si), and *p*-doped (Mg) gallium nitride. In unintentionally doped gallium nitride, at low temperature, the main thermal droop mechanism is
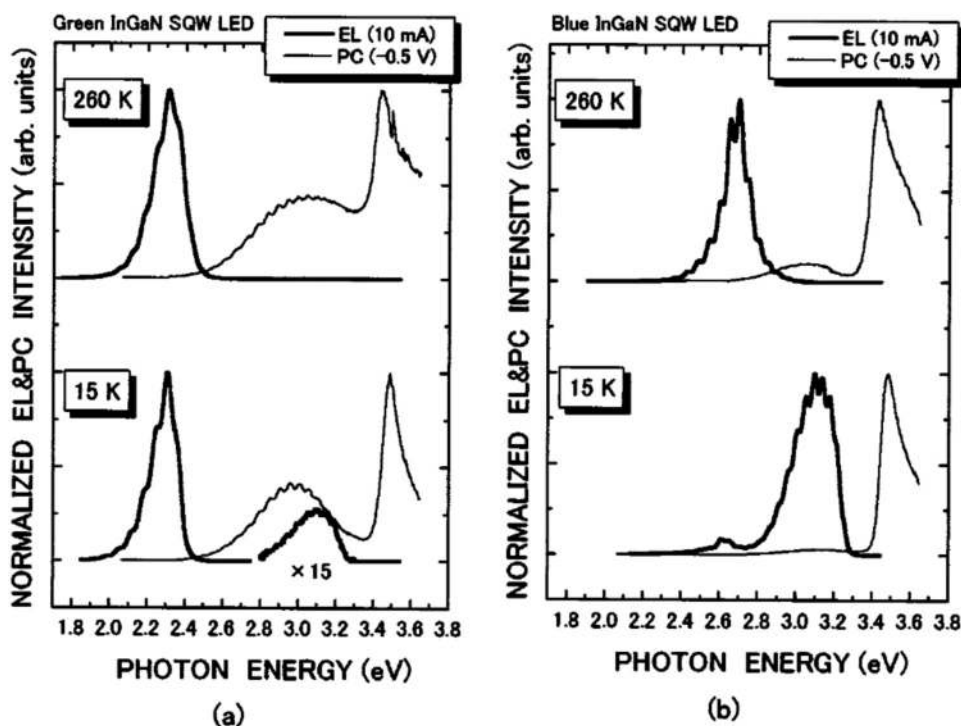

FIG. 19. Normalized EL (thick solid curves) and PC (thin solid curves) spectra of green and blue InGaN SQW LEDs at 15 and 260 K. For EL spectra, the injection current level is fixed at 10 mA, while for PC, the bias voltage is −0.5 V (reverse bias). Reprinted with permission from Hori *et al.*, J. Appl. Phys. **93**(6), 3152–3157 (2003). Copyright 2003 AIP Publishing LLC.
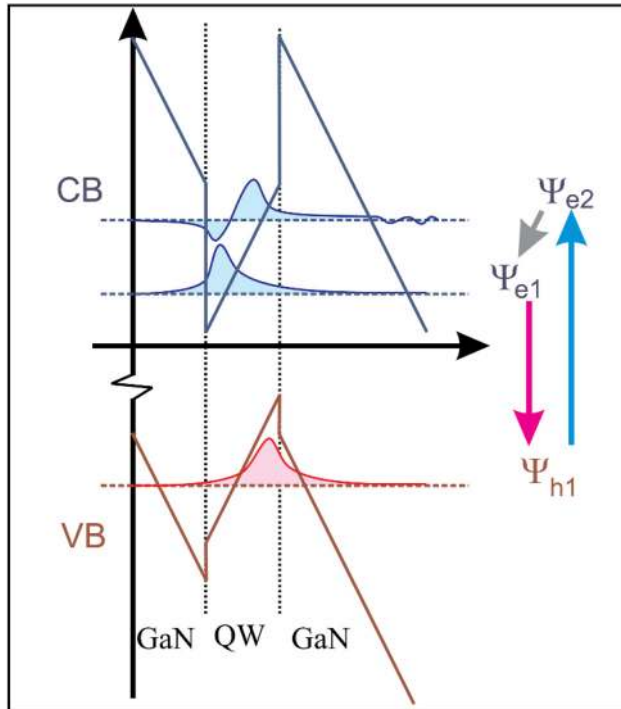
FIG. 20. The proposed scheme of states in the investigated quantum well. Reprinted with permission from Binder *et al.*, J. Appl. Phys. **114**(22), 223504 (2013). Copyright 2013 AIP Publishing LLC.

the thermal detrapping of excitons to the free exciton band, possibly from donor bound states. At higher temperature, a second process is detected, possibly caused by the ionization of the neutral donor involved in the excitonic complex or by the photoluminescence thermal quenching of the free exciton. Considering that UID GaN shows intrinsic *n*-type conductivity, the authors conclude that the origin of the thermal droop is the release of free holes, more sensitive to capture by dislocation than neutral excitons. In *n*-doped material, the authors report similar experimental results; therefore, the photoluminescence droop is again related to the recombination of neutral excitons bound to donors. In slightly *p*-doped material, the thermal detrapping of bound excitons is still present and the thermal droop activation energy is comparable to the acceptor ionization energy, suggesting that the release of free holes plays a role, as in the undoped material case. In highly *p*-doped samples, the photoluminescence droop activation energy is lower, and based on the experimental data, the authors find no conclusive explanation.

2. Trap-assisted carrier escape

In the most simple case, an increase in defect density leads to a worsening in the thermal droop due to SRH recombination, but defects can contribute to the overall optical power drop with temperature by an additional process, the trap-assisted carrier escape. This mechanism was demonstrated in Ref. 141. The authors

investigated the amount of thermal droop in five families of single-quantum-well (SQW) LEDs, differing in indium content in the quantum wells, obtained by varying the growth temperature.

The experimental results reported in Fig. 21(a) show that, in a wide experimental temperature range, the devices under test have a significant level of thermal droop, directly correlated to the density of defects detected by capacitance deep-level transient spectroscopy measurements. Since C-DLTS can only probe the region between the two positions of the edge of the space charge region corresponding to the filling and measure voltages, this technique does not provide direct information on the density of defects inside the quantum well, which cannot be crossed by the edge of the space charge region even at very low measurement temperatures.

For this reason, information on the deep-level density inside the quantum wells was obtained by means of differential carrier lifetime measurements, an independent measurement technique, that evaluates the carrier recombination rate as a function of operating current. This technique relies on the analysis of the time-dependent optical power response after an increased bias pulse to obtain the values of the A, B, and C recombination parameters.[141] In this case, the extrapolated information on the density of defects is the value of the A coefficient, larger for higher deep-level concentration. Figure 21(b) shows that the correlation between thermal droop amount and defect density is still present, regardless of the technique used to probe it or of the region probed.

The comprehensive set of measurements available allowed for the use of numerical simulations, with the goal of understanding if the detected thermal droop was caused only by SRH recombination. The simulations, reported in Fig. 22, show that the temperature variation of the non-radiative recombination lifetime, obtained by differential carrier lifetime measurements, can be closely reproduced, confirming the correct values of the simulation parameters. Surprisingly, the same set of parameters was not able to represent satisfactorily the experimental data and led to a severe underestimation, suggesting that SRH recombination alone does not account for the full thermal droop. The same conclusion can be drawn by the analysis of stress experiments: even though the A coefficient increases and photoluminescence drops during stress, the amount of thermal droop remains unchanged, proving that the two effects have a different cause.

In the literature, some papers suggest that an improvement in the thermal droop level can be obtained by adding a *p*-AlGaN electron blocking layer (EBL),[142] by using a thicker barrier,[143] or by an improved EBL structure,[144] limiting the carrier escape process described in Sec. III D 2. In order to verify the impact of carrier escape from the quantum well, several different models were tested, including thermionic emission,[145,146] phonon-assisted tunneling,[147] and thermionic trap-assisted tunneling,[148,149] but they were not able to reproduce the experimental data or to explain the detected dependence on the deep-level concentration. Therefore, a close-form model was developed, called extended thermionic trap-assisted tunneling (ETTAT) and sketched in Fig. 23(a). The model is based on two phonon-assisted tunneling processes, P1 and P2, across an intermediate deep level located in the barrier, each of them corrected to take into account the pure thermal emission at zero bias, modeled as thermionic emission from the quantum well. The full derivation and formalism of the model can be found in Ref. 141.
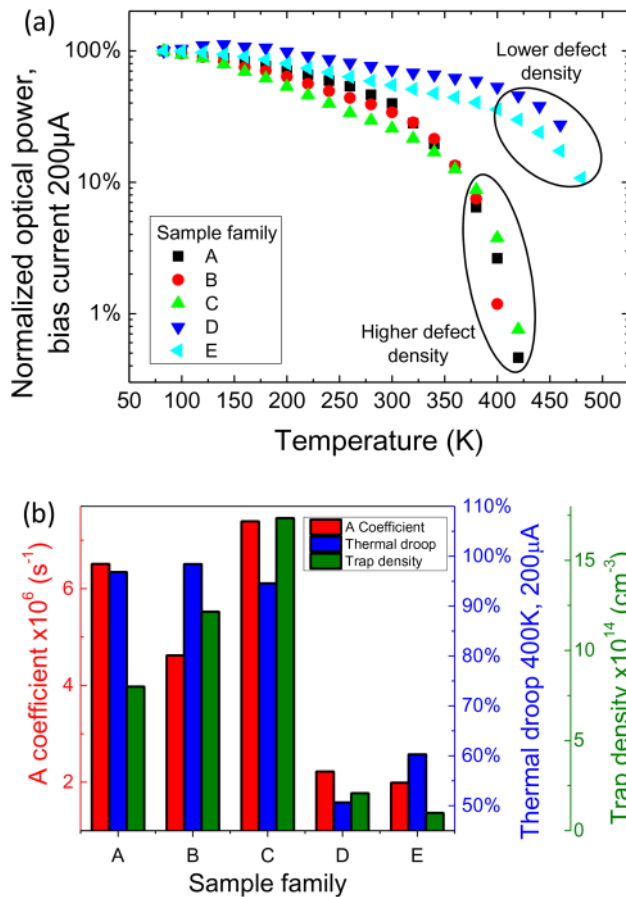
FIG. 21. (a) Optical power variation detected in SQW LEDs in a wide temperature range, for a representative 200 μA bias current. (b) The amount of thermal droop is directly correlated to the density of deep levels detected by C-DLTS and differential carrier lifetime measurements. Reprinted with permission from De Santi *et al.*, J. Appl. Phys. **119**(9), 094501 (2016). Copyright 2016 AIP Publishing LLC.
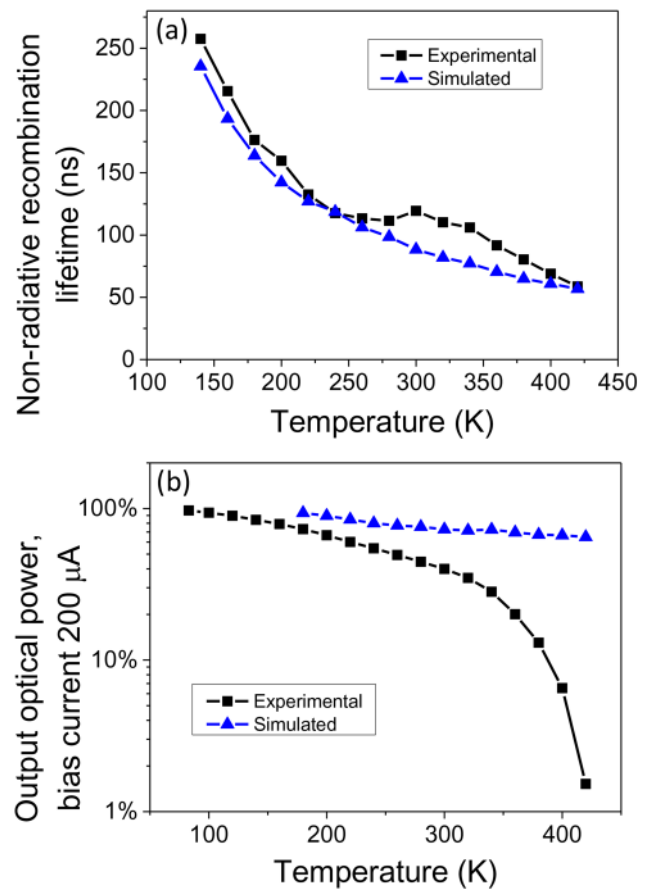

FIG. 22. (a) Numerical simulations can reproduce the experimental variation in non-radiative recombination lifetime with temperature, but (b) the same set of parameters severely underestimates the amount of thermal droop. Reprinted with permission from De Santi *et al.*, J. Appl. Phys. **119**(9), 094501 (2016). Copyright 2016 AIP Publishing LLC.

This new model is able to reproduce completely the experimental thermal droop trend, as shown in Fig. 23(b). All the relevant model parameters and intermediate deep-level positions were obtained by additional experimental measurements; the only fit parameter is the value of the electric field inside the barrier, which is not easy to determine. Figure 23(c) summarizes the different contributions in the model, showing that the thermionic emission part at zero bias accounts only for a small fraction of the overall thermal droop and is visible only at high temperature, whereas the strongest contribution comes from the phonon-assisted tunneling process.

F. Efficiency at extremely low currents

Sections III A–III E cover extensively the possible thermal droop processes occurring near the operating bias points. The

analysis of the behavior at extremely low bias (i.e., below the micro-ampere range) is often overlooked, but it can provide useful information on the current conduction processes and on the properties of defect states inside the quantum wells.[30,150] Moreover, in the last few years, the efficiency and behavior of LEDs biased at very low bias levels have been subjects of growing interest, due to the use in displays with high dynamic range and, therefore, several orders of magnitude in dimming intensity.

A complete analysis of the optical performance at extremely low current level is not an easy task due to experimental limitations, since it is difficult to collect very low levels of electroluminescence while preserving the linearity of the readout. This was done in Ref. 152 by means of a high sensitivity photodiode able to read power levels down to tens of fW, which was also used for coarse spectral analysis by using long-pass and short-pass filters, given the insufficient sensitivity of grating-based systems.
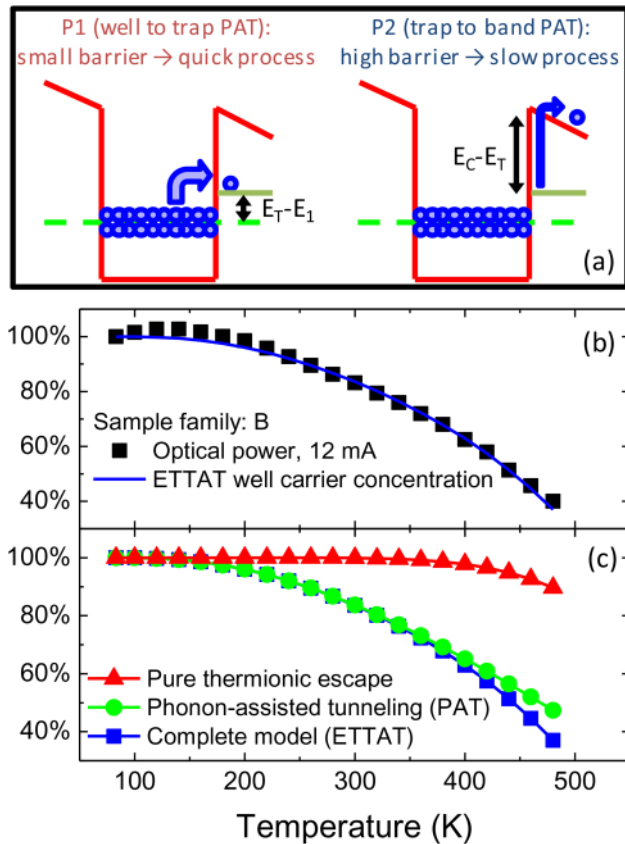
FIG. 23. (a) Sketch of the extended thermionic trap-assisted tunneling model, (b) able to fully reproduce the experimental thermal droop. (c) shows the contributions of the thermionic and of the tunneling part. Reprinted with permission from De Santi *et al.*, J. Appl. Phys. **119**(9), 094501 (2016). Copyright 2016 AIP Publishing LLC.

FIG. 24. Current–voltage characterization in the extremely low bias region. Reprinted with permission from De Santi *et al.*, Appl. Phys. Express **12**(5), 052007 (2019). Copyright 2019 The Japan Society of Applied Physics.

Figure 24 shows a high-resolution current–voltage measurement, where a clear change in slope can be observed at ≈100 nA. The value of the idiality factor in the two slope regions is 3.75 and 2.74, respectively, below and above 100 nA. A value higher than 2 is an indication that the current conduction mechanism is not charge diffusion or generation/recombination current,[32,152] confirming the important role of conduction through defect states. Additional experimental results highlight the possible presence of a resonant tunneling carrier conduction process through deep levels at higher bias levels (above 2 V).[153] At ≈100 μA, the value of the idiality factor is the lowest (1.88), suggesting the beginning of the carrier diffusion regime and the turn-on of the diode.

Figure 25(a) reports the results of the temperature-dependent optical power measurements in the extremely low bias range, highlighting several different features. In order to decouple contribution by the band-to-band recombination in the quantum wells and by deep levels, the measurement was repeated by using a 500 nm long-pass filter and a 450 nm short-pass filter, as shown in Figs. 25(b) and 25(c), respectively.
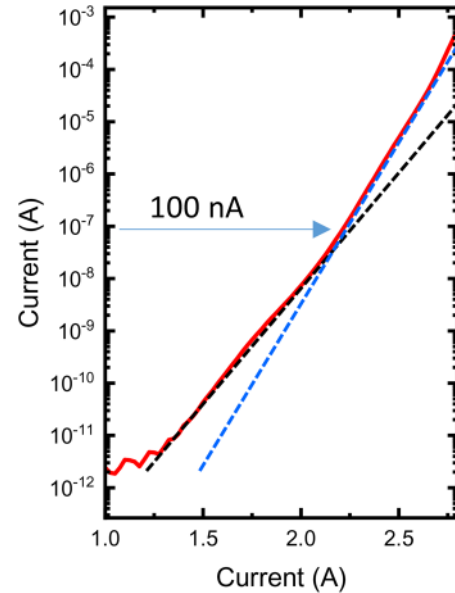
Band-to-band recombination in the quantum wells can be already detected at 10 nA. The emission intensity decreases with temperature, and the slope of the log–log L-I plot is ≈2.6 and not sensitive to temperature, suggesting that at such low current levels, the thermal droop is caused by SRH recombination.[154]

Defect-assisted emission is a well-known phenomenon in the gallium nitride material systems, notable examples being the yellow luminescence[155–159] and blue luminescence,[49,160–162] and in the case under analysis, it takes place in the full experimental range. Below 10 nA, the EL signal increases with a log–log slope from 2.27 to 1.79 when the temperature increases from 15 °C to 75 °C. The value of the slope suggests that the emission is caused by parasitic intragap transitions, and the increase in emission intensity with increasing temperature can be ascribed to the higher carrier capture rate, according to the SRH recombination theory (see Sec. II B). Above 10 nA, the optical power does not increase anymore, consistently with the saturation of the recombination through the deep levels, which are present in finite concentration. Moreover, it can be noticed that the QW emission overcomes the defect-related contribution at ≈100 nA, i.e., the current level highlighted in Fig. 24 for the transition between two different conduction modes, suggesting that the origin of the transition between different emission types is a change in the conduction mode.

The actual nature of the defect states leading to the low-bias current conduction is currently under debate, and in the literature, papers based on theoretical studies mention trap-assisted tunneling through midgap states or shallow Mg acceptors located in the quantum barriers and in the quantum wells,[150] possibly assisted by additional states in the spacer and in the electron blocking layer.[30]
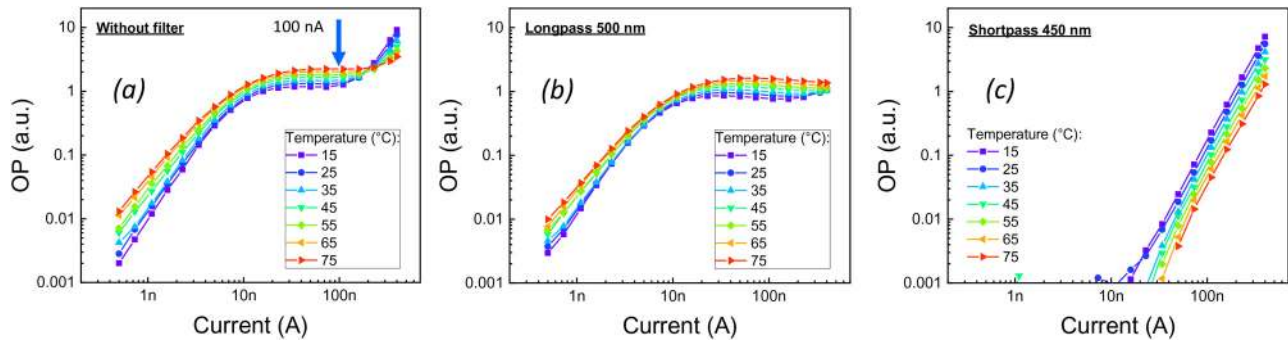
FIG. 25. (a) Full electroluminescence vs bias characterization from 15 °C to 75 °C in the extremely low bias region. It can be divided into (b) contribution from deep levels (≥500 nm) and (c) quantum well emission (≤450 nm). Reprinted with permission from Reprinted with permission from De Santi *et al.*, Appl. Phys. Express **12**(5), 052007 (2019). Copyright 2019 The Japan Society of Applied Physics.

The analysis of the spectral distribution of the electroluminescence can provide useful information on possible radiative deep-level related transitions and, therefore, on the defects involved in the current conduction process. The results of measurements carried out by using long-pass filters with various cutoff wavelengths are summarized in Figs. 26 and 29(a). The emission wavelength is longer than 1000 nm (1.24 eV). Figure 26(b) summarizes the possible tunneling and emission processes.

G. Thermal droop in UV-B LEDs

Thermally activated processes can also affect the parasitic emission bands of LEDs. Studying the temperature dependence spectral properties is especially relevant for devices where the presence of parasitic emission is the strongest, such as in UV emitters, as proposed in Ref. 104. Additional details on the samples and the fabrication process can be found in Refs. 164–166.

The complete result of the thermal droop characterization is summarized in Fig. 27, for a representative 1 mA bias current. Four different emission peaks are clearly visible, some of them (peak 3 and 4) showing as broad wavelength distribution, with different temperature and current dependencies. Peak 1 was only visible at very low current and temperature levels; therefore, it was not analyzed in the referenced work. Peak 2 corresponds to the nominal emission wavelength of the LED; therefore, it is ascribed to band-to-band recombination in the quantum wells. Peaks 3 and 4 are parasitic emission peaks, whose origin has to be understood.

For a clearer visualization, Fig. 28 shows the dependence of the peak QW emission on temperature and bias current in the full tested range where it could be measured. Three different regions are clearly visible: (i) low temperature and low bias, in blue, where the optical power decreases with temperature; (ii) low temperature and high bias, in green, where the optical power increases with
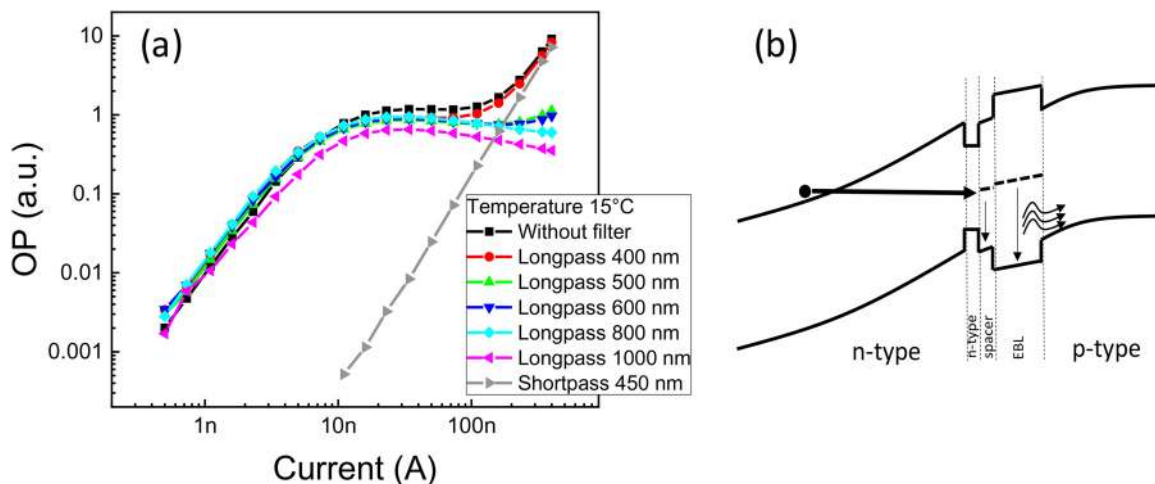

FIG. 26. (a) Tests carried out by varying long-pass filter cutoff frequency, to identify the dominant deep-level energy. (b) summarizes the possible emission processes. Reprinted with permission from De Santi *et al.*, Appl. Phys. Express **12**(5), 052007 (2019). Copyright 2019 The Japan Society of Applied Physics.
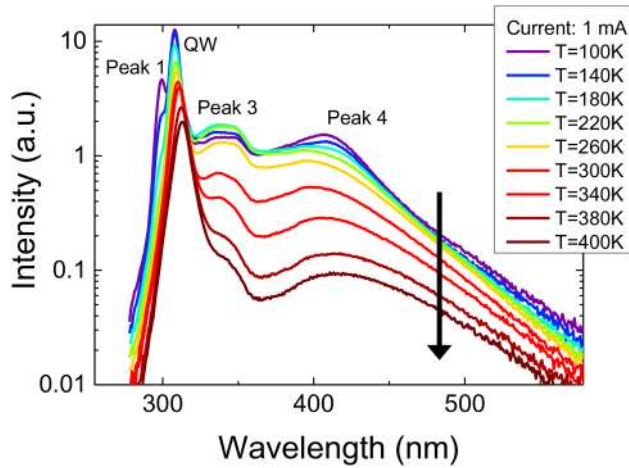
FIG. 27. Measured electroluminescence spectra of a 308 nm UV-B LED in a wide temperature range, for a representative 1 mA current level. Reprinted with permission from De Santi *et al.*, Photonics Res. **5**(2), A44–A51 (2017). Copyright 2017 CLP.

temperature; (iii) high temperature, in red, where the optical power decreases with a trend that differs from the one in region (i).

In the first region, the optical power decrease closely follows the Arrhenius law, leading to an activation energy in the range of 66–77 meV. The low value is compatible with values reported in the literature for exciton delocalization.[166–170] The comparison with the literature and the fact that the process is present at low temperature and bias levels suggest that exciton delocalization is the physical process causing the thermal droop in region (i), as described in Sec. III D 1.
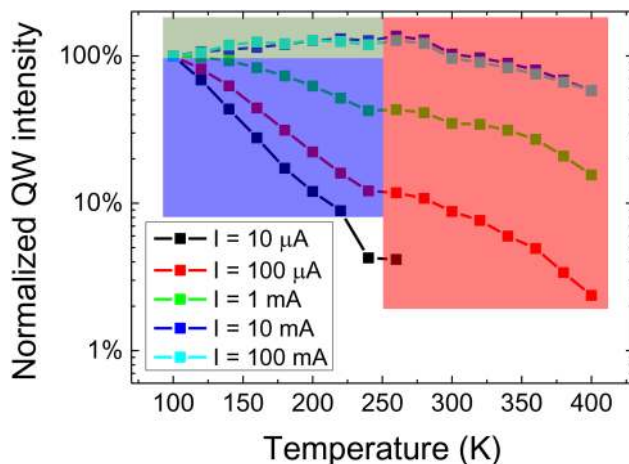

FIG. 28. Summary of the temperature and bias dependence of the quantum well peak emission. Reprinted with permission from De Santi *et al.*, Photonics Res. **5**(2), A44–A51 (2017). Copyright 2017 CLP.
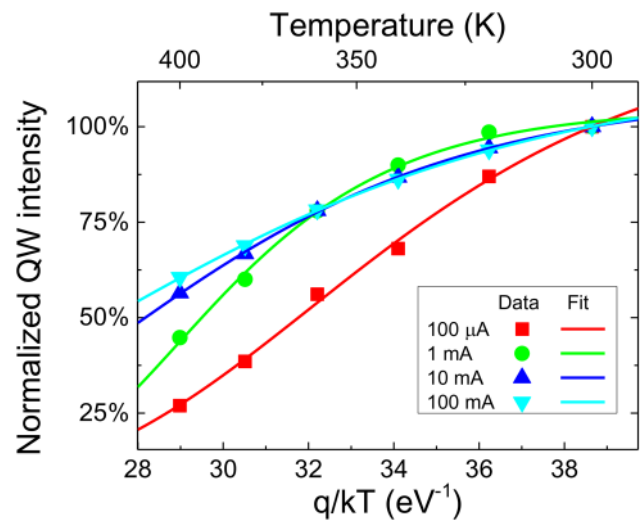

FIG. 29. Fit of the quantum well emission in the high temperature range, showing good agreement with the developed SRH closed-form model. Reprinted with permission from De Santi *et al.*, Photonics Res. **5**(2), A44–A51 (2017). Copyright 2017 CLP.

In the second region, the EL signal increases with the temperature. As discussed in Sec. II A, this effect can be caused by the improvement in carrier injection efficiency in the quantum wells, typically of holes since they are the carrier species with the lowest mobility and the highest freeze out in the gallium nitride material system. In the case under analysis, this hypothesis is confirmed by the results of numerical simulations, reported in Ref. 104. With increasing temperature, calculations show a significant improvement in the hole concentration in the quantum well farther from the *p*-side and a negligible variation in electron density, leading to the higher amount of electron–hole recombination events.

In the third region, the thermal droop at operating temperature and current levels is expected to be caused by SRH recombination (see Sec. II B), but this qualitative hypothesis has to be confirmed by a more accurate numerical modeling of the experimental data. To this aim, a closed-form model was developed, based on the equation for the temperature dependence of the nonradiative lifetime in the Shockley–Read–Hall model [Eq. (5)] and on the ABC rate equation. Thanks to the former, it is possible to obtain information on the energy position of the deep level inside the bandgap, since the value of the activation energy is a fitting parameter. The latter is often used in the literature for the analysis of the dependence of the efficiency of an optoelectronic device on recombination parameters and carrier concentration. The full derivation of the model is reported in Ref. 104, and Fig. 29 shows the fit results on top of the experimental data in the range under analysis. The extrapolated values of the deep-level energy are in the range of 165–342 meV from the intrinsic Fermi level. The good agreement confirms numerically and with device physics backing that the thermal droop in region 3 is indeed caused by the increase in SRH recombination caused by a deep level located close to midgap.
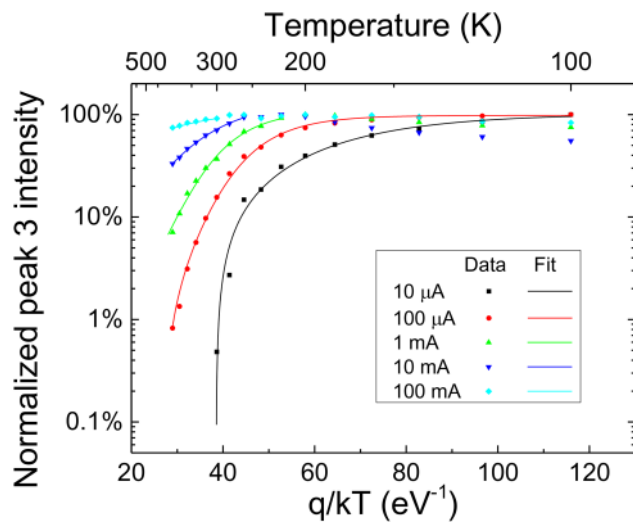
FIG. 30. Summary of the temperature and bias dependence of peak 3 emission, including fit according to the SRH model. Reprinted with permission from De Santi *et al.*, Photonics Res. **5**(2), A44–A51 (2017). Copyright 2017 CLP.

The analysis of peak 3 in Fig. 27 is based on the same model, and the results of the fit on peak 3 maximum intensity is reported in Fig. 30. By comparing the experimental data with the ones in Fig. 27, it can be noticed that the difference in slope leading to the identification of regions (i) and (iii) is not present anymore, suggesting that peak 3 emission does not originate from the QWs since no exciton delocalization is visible. The fit according to the novel SRH model is of good quality, confirming that the physical
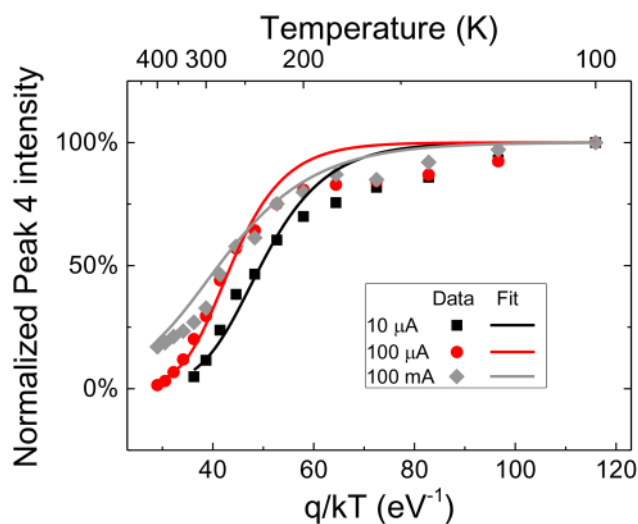

FIG. 31. Summary of the temperature and bias dependence of peak 4 emission, including fit according to the SRH model. Reprinted with permission from De Santi *et al.*, Photonics Res. **5**(2), A44–A51 (2017). Copyright 2017 CLP.

cause of the thermal droop is SRH recombination. Moreover, at low temperature and high bias, the increase in EL intensity already discussed for the QW peak is still visible, indicating that the layer where the radiative recombination is occurring has to be located in the intrinsic or *n*-type region of the device, since it is influenced by hole injection efficiency. The broad shape of peak 3 suggests that the emission is caused by parasitic radiative recombination assisted by deep levels, and by analyzing all the collected information in a consistent way, we can conclude that the layer originating peak 3 EL is the quantum barrier next to the EBL. The aforementioned numerical simulations show a high electron–hole pair concentration in that region, further supporting the identification of the device layer responsible for peak 3 emission.

In the case of peak 4, the broad spectral shape suggests a defect-related radiative transition. The experimental data summarized in Fig. 31 show that no effect of the increase in hole injection efficiency is present, pointing out that the emission takes place in the *p*-side of the device. The model is not able to reproduce the experimental data, suggesting that SRH recombination alone is not the cause of the detected trend and that additional mechanisms (such as carrier transport effects) can influence the thermal droop of peak 4. The wavelength value suggests as the possible originating layer the AlGaN/AlGaN short-period superlattice (SPSL) in the *p*-side, which is the region where carrier transport effects should have the strongest impact.

In order to achieve a complete modeling of the optical behavior in the full temperature and bias range under analysis, additional effects have to be taken into account, such as the temperature variation of the *B* coefficient discussed in Sec. III C.

IV. HOW TO MINIMIZE THERMAL DROOP?

After an extensive discussion on the physical mechanisms responsible for thermal droop, we discuss how simple design choices can be adopted to mitigate thermal droop. This has to be intended more as an intuitive discussion, rather than a quantitative assessment of the possible remedies to thermal droop (that can be the subject of future technical publications on this topic).

To minimize thermal droop, one can work both at the device and at the system level, as schematically summarized in Fig. 32: at device level, to make the structure less sensitive to temperature-induced losses; at system levels, to minimize device operating temperature, through proper optimization of the driving conditions and of the heat sink components.

At device level, it is clear that the amount of thermal droop depends on the interplay of several microscopic processes that take place in/near the active region and change the rates of carrier injection and recombination. Based on the discussion above, one can consider the existence of processes of different natures, as briefly summarized in the following.

Injection/escape-related processes: These are processes that limit the injection efficiency with increasing temperature. This group includes carrier escape (a thermionic process, which is exponentially dependent on the height of the confinement barrier and on the operating temperature), carrier overflow (related to the increase in the position of the Fermi level above the conduction band energy, and strictly dependent on bias conditions and on the height of the
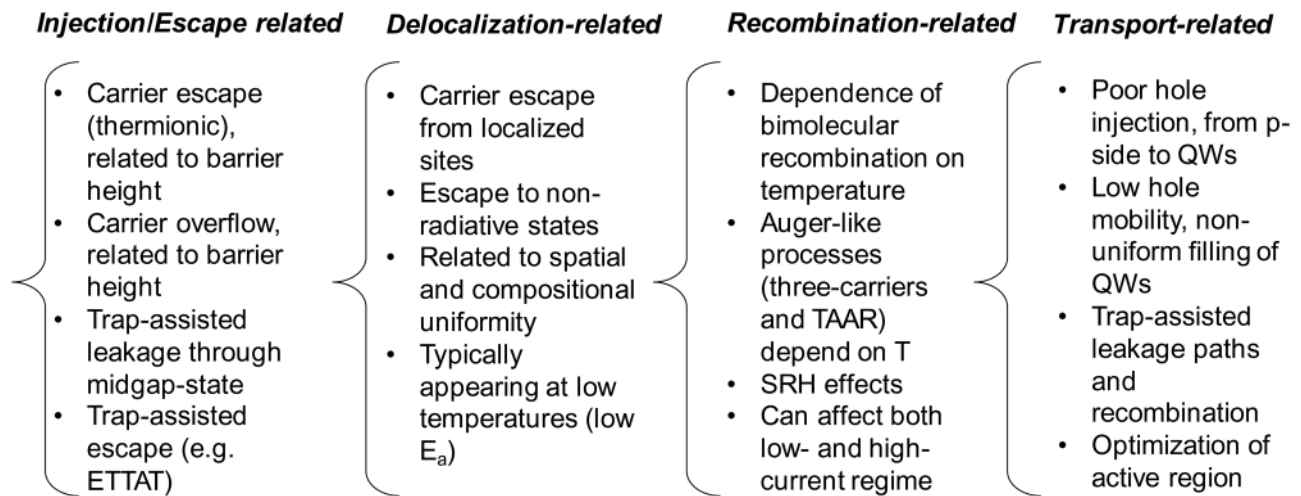
FIG. 32. Summary of the main processes responsible for thermal droop, as described in this paper.

confinement barrier); trap-assisted leakage processes. As an example of the latter, we mention here trap-assisted tunneling through midgap states (as described by Refs. 30 and 151) that favors carrier leakage at low current levels, and extended thermionic trap-assisted tunneling (ETTAT), consisting in two phonon-assisted tunneling processes, P1 and P2, across an intermediate deep level located in the barrier. To minimize the thermal droop related to these mechanisms, one needs to act on the microscopic structure of the active region. Specifically, by increasing the conduction band discontinuity between the QWs and the barrier, it is possible to substantially reduce the escape and overflow components. In this respect, III-nitrides offer a much greater flexibility compared to phosphide-based LEDs, and typical visible LEDs have barriers greater than 0.2–0.3 eV, thus resulting in relatively low escape and overflow components at nominal current/temperature conditions. With regard to trap-assisted leakage processes, they can be minimized through a careful optimization of the quality of the semiconductor. In this direction, a reduction of threading dislocation density below $10^7 \, cm^{-2}$ can be beneficial,[171] but attention has to be also on point defect density. Specifically, the density of midgap states related to point defects needs to be minimized in order to reduce the defect-related leakage components. Details on how the properties of midgap states impact on carrier leakage can be found in Refs. 30 and 151.

Delocalization-related processes: The contribution of carrier de-localization typically appears at low temperature and/or low injection levels. Once carriers exit the localized states, they can move through the semiconductor and reach non-radiative recombination sites. This process typically has a low activation energy (few tens of eV), since the height of the confining potential is relatively low. To minimize the effects of these processes, it can be important to improve both the spatial and compositional uniformity of the material to reduce the existence of localization sites and the height of the related confinement barriers. In addition, to minimize the probability of SRH recombination after carriers escape the

localization site, the density of defects should be minimized [below $10^{14} \, cm^{-3}$ (Ref. 141)], in order to improve thermal stability.

Recombination-related processes: Once carriers are injected in the quantum wells, several recombination processes compete, and all the recombination rates have a significant temperature dependence. Specifically, the radiative recombination rate decreases with temperature, thus resulting in a drop in radiative recombination efficiency, according to $B(T) = B_0 T^{-3/2}$.[88] Recent studies on high-quality InGaN single-quantum-well LEDs suggest that, at low current, the B coefficient decreases with the temperature due to Coulomb interaction between electrons and holes; at high current, B can increase due to the screening of the internal field, which increases the electron–hole wavefunction overlap.[25] Also, the Auger recombination coefficient varies with increasing temperature, following the exponential law described in (12), and this can impact on the thermal droop at high carrier densities.[54,91] In addition, recent papers indicated that defect-related Auger-like processes (TAAR) can further contribute to carrier losses at high carrier densities.[17,58] To minimize high-order losses, one needs to increase the recombination volume, e.g., by increasing quantum well thickness, or by using multiple quantum wells, instead of a single-quantum-well layout. When doing this, one needs to consider a couple of trade-offs. In fact, when increasing the width of the quantum wells, the overlap between the electron and hole wavefunction decreases, due to the quantum-confined Stark effect, and this effect is particularly strong at low carrier densities. When increasing the number of quantum wells, one needs to consider the difficulty of injecting holes from the p-side, both due to the existence of energy barriers and to the lower mobility of positively charged carriers. At low current levels, the effects of Shockley–Read–Hall recombination become relevant. As widely discussed in Sec. III, the only remedy against SRH recombination is a general improvement in material quality, with the aim of decreasing the SRH recombination rate below $10^5 \, s^{-1}$, to minimize the SRH components.[25]

Transport-related processes: As extensively described above, thermal droop can be influenced by the temperature dependence of transport mechanisms. A first process is related to the difficult hole injection from the p-side to the quantum wells.[75] This can be related to the existence of potential barriers between the p-GaN, the electron blocking layer, and the n-type semiconductor. A careful optimization of the band structure and doping of the EBL can improve the injection of holes, thus improving the stability of the electrical and optical characteristics with increasing temperature. A second factor to be considered is the relatively low hole mobility that may lead to a non-uniform filling of the quantum wells.[104] Here, the parameter design space includes the distance of the quantum wells from the p-GaN, the width of the barriers between the wells, and the number of quantum wells. Finally, defects can favor tunneling processes that—as already discussed—can favor the creation of leakage/escape paths.[140]

With regard to the system-level remedies to thermal droop, one needs to consider all possible ways to minimize the temperature reached by the device during operation. First, with regard to the driving strategy, two different approaches are typically used to control the light output of LEDs, namely, constant current mode (CCM) and pulse width modulation (PWM). The latter ensures a much better linearity, especially at low current levels, since the optical output is determined by the duty cycle of the driving waveform and not by the (not-ideally linear) dependence between optical power and current. However, it has to be considered that during PWM operation, the LEDs are driven at much higher peak current, compared to what would be needed in CCM for the same optical power. As a consequence, non-radiative (Auger-like) and resistive losses may be higher in PWM, and this may result in increased self-heating, compared to CCM. In this respect, CCM would be a preferable choice to minimize self-heating and improve the temperature-stability of LEDs. A second consideration deals with the design of the heat dissipation system. The thermal resistance of 1 A LEDs can be in the order of 8–10 K/W,[172] on a very small footprint ($<10\,mm^2$). In case several LEDs are used in a closely spaced array, the thermal resistance of the illuminator can be minimized through the use of metal-core printed circuit boards (MC-PCBs) with a thermally conductive base material, like aluminum or copper. For these boards, the critical parameters are the thickness and the thermal conductivity of the dielectric material used to electrically isolate the LED from the heat sink. Very thin dielectrics ($<40\,\mu m$) can reach thermal conductivity above 7 W/mK[173] thus permitting a high density integration of LED arrays. Then, if a passive heat sink is not sufficient to ensure a low operating temperature, active cooling strategies (either with a fan or a liquid system) should be considered. In any case, for the development of high-flux applications, it is of fundamental importance to directly estimate the junction temperature of the devices in the real operation environment, e.g., through the forward voltage method[174] or through an analysis of the wavelength shift.[175]

V. CONCLUSIONS

Several processes can contribute to the thermal droop, thus resulting in a significant decrease in the internal quantum efficiency of III-nitride based LEDs at high temperature levels. In several cases,

the analysis of the underlying processes is not straightforward, since both recombination-related processes (e.g., changes in the recombination coefficients) and transport-related phenomena (including carrier delocalization and escape) can contribute.

In this paper, we have summarized the most relevant processes responsible for the thermal droop in nitride-based LEDs, the related physics, and their dependence on temperature. A critical discussion on the literature in the field has also been presented to help the reader approaching this interesting and challenging topic. From the results presented in this paper, it is clear that most of the thermal droop mechanisms can be minimized, and this results in an interesting research opportunity.

An accurate optimization of device structure is required in order to achieve high performance at high temperatures. This requires specific optimization of the doping levels and profiles (to favor injection efficiency and to balance electron and hole densities in the quantum wells), crystal quality (to minimize SRH processes and related Auger losses), heterostructure design (to minimize carrier escape), quantum well growth, and properties (to reduce losses at high temperatures and to control delocalization processes).

DATA AVAILABILITY

The data that support the findings of this study are available from the corresponding author upon reasonable request.

REFERENCES

[1] Figures from commercially available LED datasheets: Cree XHP70, Osram LUW HWQP, Nichia NVSL219CT, Samsung LH351B, and LedEngin LZP-00CW0R.

[2] S. Nakamura, M. Senoh, and T. Mukai, "P-GaN/N-InGaN/N-GaN double-heterostructure blue-light-emitting diodes," Jpn. J. Appl. Phys. **32**(Part 2, No.1A/B), L8–L11 (1993).

[3] A. David, N. G. Young, C. Lund, and M. D. Craven, "Review—The physics of recombinations in III-nitride emitters," ECS J. Solid State Sci. Technol. **9**(1), 016021 (2020).

[4] W. Liu, J.-F. Carlin, N. Grandjean, B. Deveaud, and G. Jacopin, "Exciton dynamics at a single dislocation in GaN probed by picosecond time-resolved cathodoluminescence," Appl. Phys. Lett. **109**(4), 042101 (2016).

[5] S. D. Lester, F. A. Ponce, M. G. Craford, and D. A. Steigerwald, "High dislocation densities in high efficiency GaN-based light-emitting diodes," Appl. Phys. Lett. **66**(10), 1249–1251 (1995).

[6] J. Yu, Z. Hao, L. Li, L. Wang, Y. Luo, J. Wang, C. Sun, Y. Han, B. Xiong, and H. Li, "Influence of dislocation density on internal quantum efficiency of GaN-based semiconductors," AIP Adv. **7**(3), 035321 (2017).

[7]T. Hino, S. Tomiya, T. Miyajima, K. Yanashima, S. Hashimoto, and M. Ikeda, "Characterization of threading dislocations in GaN epitaxial layers," Appl. Phys. Lett. **76**(23), 3421–3423 (2000).

[8]Y. Narukawa, Y. Kawakami, M. Funato, S. Fujita, S. Fujita, and S. Nakamura, "Role of self-formed InGaN quantum dots for exciton localization in the purple laser diode emitting at 420 nm," Appl. Phys. Lett. **70**(8), 981–983 (1997).

[9]M. J. Galtrey, R. A. Oliver, M. J. Kappers, C. J. Humphreys, D. J. Stokes, P. H. Clifton, and A. Cerezo, "Three-dimensional atom probe studies of an $In_xGa_{1-x}N$/GaN multiple quantum well structure: Assessment of possible indium clustering," Appl. Phys. Lett. **90**(6), 061903 (2007).

[10]S. F. Chichibu, A. Uedono, T. Onuma, B. A. Haskell, A. Chakraborty, T. Koyama, P. T. Fini, S. Keller, S. P. DenBaars, J. S. Speck, U. K. Mishra, S. Nakamura, S. Yamaguchi, S. Kamiyama, H. Amano, I. Akasaki, J. Han, and T. Sota, "Origin of defect-insensitive emission probability in In-containing (Al, In,Ga)N alloy semiconductors," Nat. Mater. **5**(10), 810–816 (2006).

[11]T. Takeuchi, S. Sota, M. Katsuragawa, M. Komori, H. Takeuchi, H. Amano, and I. Akasaki, "Quantum-confined Stark effect due to piezoelectric fields in GaInN strained quantum wells," Jpn. J. Appl. Phys. **36**(Part 2, No. 4A), L382–L385 (1997).

[12]S. Karpov, "ABC-model for interpretation of internal quantum efficiency and its droop in III-nitride LEDs: A review," Opt. Quantum Electron. **47**(6), 1293–1303 (2015).

[13]Ü. Ozgur, H. Liu, X. Li, X. Ni, and H. Morkoç, "GaN-based light-emitting diodes: Efficiency at high injection levels," Proc. IEEE **98**(7), 1180–1196 (2010).

[14]G. Verzellesi, D. Saguatti, M. Meneghini, F. Bertazzi, M. Goano, G. Meneghesso, and E. Zanoni, "Efficiency droop in InGaN/GaN blue light-emitting diodes: Physical mechanisms and remedies," J. Appl. Phys. **114**(7), 071101 (2013).

[15]C. Weisbuch, "Review—On the search for efficient solid state light emitters: Past, present, future," ECS J. Solid State Sci. Technol. **9**(1), 016022 (2020).

[16]H. Fu and Y. Zhao, *Efficiency Droop in GaInN/GaN LEDs* (Elsevier, 2018), pp. 299–325.

[17]A. David, N. G. Young, C. A. Hurni, and M. D. Craven, "Quantum efficiency of III-nitride emitters: Evidence for defect-assisted nonradiative recombination and its effect on the green gap," Phys. Rev. Appl. **11**(3), 031001 (2019).

[18]A. David and M. J. Grundmann, "Efficiency droop in III-nitride LEDs: Overview and carrier lifetime analysis," in *Numerical Simulation of Optoelectronic Devices, Atlanta, GA, 6–9 September 2010* (IEEE, 2010), pp. 87–88.

[19]A. David and M. J. Grundmann, "Droop in InGaN light-emitting diodes: A differential carrier lifetime analysis," Appl. Phys. Lett. **96**(10), 103504 (2010).

[20]B. Galler, H.-J. Lugauer, M. Binder, R. Hollweck, Y. Folwill, A. Nirschl, A. Gomez-Iglesias, B. Hahn, J. Wagner, and M. Sabathil, "Experimental determination of the dominant type of Auger recombination in InGaN quantum wells," Appl. Phys. Express **6**(11), 112101 (2013).

[21]A. C. Espenlaub, A. I. Alhassan, S. Nakamura, C. Weisbuch, and J. S. Speck, "Auger-generated hot carrier current in photo-excited forward biased single quantum well blue light emitting diodes," Appl. Phys. Lett. **112**(14), 141106 (2018).

[22]I. E. Titkov, S. Y. Karpov, A. Yadav, V. L. Zerova, M. Zulonas, B. Galler, M. Strassburg, I. Pietzonka, H. J. Lugauer, and E. U. Rafailov, "Temperature-dependent internal quantum efficiency of blue high-brightness light-emitting diodes," IEEE J. Quantum Electron. **50**(11), 911–920 (2014).

[23]L. Zhao, D. Yan, Z. Zhang, B. Hua, G. Yang, Y. Cao, E. X. Zhang, X. Gu, and D. M. Fleetwood, "Temperature-dependent efficiency droop in GaN-based blue LEDs," IEEE Electron Device Lett. **39**(4), 528–531 (2018).

[24]Y. Zhao, H. Fu, G. T. Wang, and S. Nakamura, "Toward ultimate efficiency: Progress and prospects on planar and 3D nanostructured nonpolar and semipolar InGaN light-emitting diodes," Adv. Opt. Photonics **10**(1), 246 (2018).

[25]A. David, N. G. Young, C. Lund, and M. D. Craven, "Thermal droop in high-quality InGaN LEDs," Appl. Phys. Lett. **115**(22), 223502 (2019).

[26]N. Grandjean, J. Massies, I. Grzegory, and S. Porowski, "Gan/AlGaN quantum wells for UV emission: Heteroepitaxy versus homoepitaxy," Semicond. Sci. Technol. **16**(5), 358–361 (2001).

[27]See https://www.cree.com/led-components/media/documents/ds-XQE.pdf for "Cree ® XLamp ® XQ-E LEDs" (2018).

[28]M. Vallone, M. Goano, F. Bertazzi, and G. Ghione, "Carrier capture in InGaN/GaN quantum wells: Role of electron-electron scattering," J. Appl. Phys. **121**(12), 123107 (2017).

[29]D. S. Meyaard, G. B. Lin, J. Cho, E. F. Schubert, H. Shim, S. H. Han, M. H. Kim, C. Sone, and Y. Sun Kim, "Identifying the cause of the efficiency droop in GaInN light-emitting diodes by correlating the onset of high injection with the onset of the efficiency droop," Appl. Phys. Lett. **102**(25), 251114 (2013).

[30]M. Mandurrino, G. Verzellesi, M. Goano, M. Vallone, F. Bertazzi, G. Ghione, M. Meneghini, G. Meneghesso, and E. Zanoni, "Physics-based modeling and experimental implications of trap-assisted tunneling in InGaN/GaN light-emitting diodes," Phys. Status Solidi A **212**(5), 947–953 (2015).

[31]L. A. Coldren, S. W. Corzine, and M. L. Mašanović, *Diode Lasers and Photonic Integrated Circuits*, 2nd ed. (John Wiley & Sons, Inc., Hoboken, NJ, 2012).

[32]E. F. Schubert, *Light-Emitting Diodes* (Cambridge University Press, Cambridge, 2006).

[33]H. Zhao, G. Liu, J. Zhang, R. A. Arif, and N. Tansu, "Analysis of internal quantum efficiency and current injection efficiency in III-nitride light-emitting diodes," J. Disp. Technol. **9**(4), 212–225 (2013).

[34]M. Ikeda, F. Zhang, R. Zhou, J. Liu, S. Zhang, A. Tian, P. Wen, L. Zhang, D. Li, and H. Yang, "Thermionic emission of carriers in InGaN/(In)GaN multiple quantum wells," Jpn. J. Appl. Phys. **58**(SC), SCCB03 (2019).

[35]K. J. Vampola, M. Iza, S. Keller, S. P. DenBaars, and S. Nakamura, "Measurement of electron overflow in 450 nm InGaN light-emitting diode structures," Appl. Phys. Lett. **94**(6), 2007–2010 (2009).

[36]J. Iveland, L. Martinelli, J. Peretti, J. S. Speck, and C. Weisbuch, "Direct measurement of Auger electrons emitted from a semiconductor light-emitting diode under electrical injection: Identification of the dominant mechanism for efficiency droop," Phys. Rev. Lett. **110**(17), 177406 (2013).

[37]R. N. Hall, "Electron-hole recombination," Phys. Rev. B **87**, 387 (1952).

[38]W. Shockley and W. T. Read, "Statistics of the recombination of holes and electrons," Phys. Rev. **87**(46), 835–842 (1952).

[39]M. La Grassa, M. Meneghini, C. De Santi, M. Mandurrino, M. Goano, F. Bertazzi, R. Zeisel, B. Galler, G. Meneghesso, and E. Zanoni, "Ageing of InGaN-based LEDs: Effects on internal quantum efficiency and role of defects," Microelectron. Reliab. **55**(9–10), 1775–1778 (2015).

[40]O. Pursiainen, N. Linder, A. Jaeger, R. Oberschmid, and K. Streubel, "Identification of aging mechanisms in the optical and electrical characteristics of light-emitting diodes," Appl. Phys. Lett. **79**(18), 2895–2897 (2001).

[41]D. Monti, M. Meneghini, C. De Santi, G. Meneghesso, E. Zanoni, J. Glaab, J. Rass, S. Einfeldt, F. Mehnke, J. Enslin, T. Wernicke, and M. Kneissl, "Defect-related degradation of AlGaN-based UV-B LEDs," IEEE Trans. Electron Devices **64**(1), 200–205 (2017).

[42]S. Y. Karpov, "Effect of carrier localization on recombination processes and efficiency of InGaN-based LEDs operating in the 'green gap'," Appl. Sci. **8**(5), 818 (2018).

[43]M. Meneghini, M. la Grassa, S. Vaccari, B. Galler, R. Zeisel, P. Drechsel, B. Hahn, G. Meneghesso, and E. Zanoni, "Characterization of the deep levels responsible for non-radiative recombination in InGaN/GaN light-emitting diodes," Appl. Phys. Lett. **104**(11), 113505 (2014).

[44]C. E. Dreyer, A. Alkauskas, J. L. Lyons, J. S. Speck, and C. G. Van de Walle, "Gallium vacancy complexes as a cause of Shockley-Read-Hall recombination in III-nitride light emitters," Appl. Phys. Lett. **108**(14), 141101 (2016).

[45]E. C. Young, N. Grandjean, T. E. Mates, and J. S. Speck, "Calcium impurity as a source of non-radiative recombination in (In,Ga)N layers grown by molecular beam epitaxy," Appl. Phys. Lett. **109**(21), 212103 (2016).

[46]C. Haller, J.-F. Carlin, G. Jacopin, W. Liu, D. Martin, R. Butté, and N. Grandjean, "GaN surface as the source of non-radiative defects in InGaN/GaN quantum wells," Appl. Phys. Lett. **113**(11), 111106 (2018).

[47]P. Kessler, K. Lorenz, S. M. C. Miranda, J. G. Correia, K. Johnston, and R. Vianden, "An In-defect complex as a possible explanation for high luminous

efficacy of InGaN and AlInN based devices," Hyperfine Interact. **197**(1), 187–191 (2010).

[48] A. Terentjevs, A. Catellani, and G. Cicero, "Nitrogen vacancies at InN (11̄00) surfaces: A theoretical study," Appl. Phys. Lett. **96**(17), 171901 (2010).

[49] S. F. Chichibu, A. Uedono, K. Kojima, H. Ikeda, K. Fujito, S. Takashima, M. Edo, K. Ueno, and S. Ishibashi, "The origins and properties of intrinsic non-radiative recombination centers in wide bandgap GaN and AlGaN," J. Appl. Phys. **123**(16), 161413 (2018).

[50] A. M. Armstrong, B. N. Bryant, M. H. Crawford, D. D. Koleske, S. R. Lee, and J. J. Wierer, "Defect-reduction mechanism for improving radiative efficiency in InGaN/GaN light-emitting diodes using InGaN underlayers," J. Appl. Phys. **117**(13), 134501 (2015).

[51] B. Galler, P. Drechsel, R. Monnard, P. Rode, P. Stauss, S. Froehlich, W. Bergbauer, M. Binder, M. Sabathil, B. Hahn, and J. Wagner, "Influence of indium content and temperature on Auger-like recombination in InGaN quantum wells grown on (111) silicon substrates," Appl. Phys. Lett. **101**, 131111 (2012).

[52] J. Piprek, "Efficiency droop in nitride-based light-emitting diodes," Phys. Status Solidi A **207**(10), 2217–2225 (2010).

[53] S. Chiaria, E. Furno, M. Goano, and E. Bellotti, "Design criteria for near-ultraviolet GaN-based light-emitting diodes," IEEE Trans. Electron Devices **57**(1), 60–70 (2010).

[54] J. Hader, J. V. Moloney, and S. W. Koch, "Temperature dependence of radiative and Auger losses in quantum wells," IEEE J. Quantum Electron. **44**(2), 185–191 (2008).

[55] K. T. Delaney, P. Rinke, and C. G. Van de Walle, "Auger recombination rates in nitrides from first principles," Appl. Phys. Lett. **94**(19), 191109 (2009).

[56] F. Bertazzi, M. Goano, and E. Bellotti, "A numerical study of Auger recombination in bulk InGaN," Appl. Phys. Lett. **97**(23), 12–15 (2010).

[57] E. Kioupakis, D. Steiauf, P. Rinke, K. T. Delaney, and C. G. Van De Walle, "First-principles calculations of indirect Auger recombination in nitride semiconductors," Phys. Rev. B **92**(3), 035207 (2015).

[58] A. C. Espenlaub, D. J. Myers, E. C. Young, S. Marcinkevičius, C. Weisbuch, and J. S. Speck, "Evidence of trap-assisted Auger recombination in low radiative efficiency MBE-grown III-nitride LEDs," J. Appl. Phys. **126**(18), 184502 (2019).

[59] Y. C. Shen, G. O. Mueller, S. Watanabe, N. F. Gardner, A. Munkholm, and M. R. Krames, "Auger recombination in InGaN measured by photoluminescence," Appl. Phys. Lett. **91**(14), 141101 (2007).

[60] A. Laubsch, M. Sabathil, J. Baur, M. Peter, and B. Hahn, "High-power and high-efficiency InGaN-based light emitters," IEEE Trans. Electron Devices **57**(1), 79–87 (2010).

[61] M. Meneghini, N. Trivellin, G. Meneghesso, E. Zanoni, U. Zehnder, and B. Hahn, "A combined electro-optical method for the determination of the recombination parameters in InGaN-based light-emitting diodes," J. Appl. Phys. **106**(11), 114508 (2009).

[62] H. Y. Ryu, D. S. Shin, and J. I. Shim, "Analysis of efficiency droop in nitride light-emitting diodes by the reduced effective volume of InGaN active material," Appl. Phys. Lett. **100**(13), 131109 (2012).

[63] A. David, M. J. Grundmann, J. F. Kaeding, N. F. Gardner, T. G. Mihopoulos, and M. R. Krames, "Carrier distribution in (0001)InGaN/GaN multiple quantum well light-emitting diodes," Appl. Phys. Lett. **92**(5), 053502 (2008).

[64] J. Hader, J. V. Moloney, and S. W. Koch, "Density-activated defect recombination as a possible explanation for the efficiency droop in GaN-based light emitters," in *2011 Conference on Lasers and Electro-Optics Europe and 12th European Quantum Electronics Conference (CLEO EUROPE/EQEC), Munich, Germany, 22–26 May 2011* (IEEE, 2011), CB7_1.

[65] J. Hader, J. V. Moloney, B. Pasenow, S. W. Koch, M. Sabathil, N. Linder, and S. Lutgen, "On the importance of radiative and Auger losses in GaN-based quantum wells," Appl. Phys. Lett. **92**(26), 261103 (2008).

[66] M. Auf Der Maur, A. Pecchia, G. Penazzi, W. Rodrigues, and A. Di Carlo, "Efficiency drop in green InGaN/GaN light emitting diodes: The role of random alloy fluctuations," Phys. Rev. Lett. **116**(2), 027401 (2016).

[67] C.-K. Li, M. Piccardo, L.-S. Lu, S. Mayboroda, L. Martinelli, J. Peretti, J. S. Speck, C. Weisbuch, M. Filoche, and Y.-R. Wu, "Localization landscape theory of disorder in semiconductors. III. Application to carrier transport and recombination in light emitting diodes," Phys. Rev. B **95**(14), 144206 (2017).

[68] M. Filoche and S. Mayboroda, "Universal mechanism for Anderson and weak localization," Proc. Natl. Acad. Sci. U. S. A. **109**(37), 14761–14766 (2012).

[69] C. Huh, W. J. Schaff, L. F. Eastman, and S. J. Park, "Temperature dependence of performance of InGaN/GaN MQW LEDs with different indium compositions," IEEE Electron Device Lett. **25**(2), 61–63 (2004).

[70] J. S. Hwang, A. Gokarna, Y.-H. Cho, J. K. Son, S. N. Lee, T. Sakong, H. S. Paek, O. H. Nam, Y. Park, and S. H. Park, "Comparative investigation of InGaN quantum well laser diode structures grown on freestanding GaN and sapphire substrates," J. Appl. Phys. **102**(1), 013508 (2007).

[71] S. Chhajed, J. Cho, E. F. Schubert, J. K. Kim, D. D. Koleske, and M. H. Crawford, "Temperature-dependent light-output characteristics of GaInN light-emitting diodes with different dislocation densities," Phys. Status Solidi A **208**(4), 947–950 (2011).

[72] C. K. Wang, Y. Z. Chiou, and D. J. Sun, "The hot-cold effect on optical properties for nitride-based green LEDs by ammonia source preflow," ECS J. Solid State Sci. Technol. **2**(7), Q104–Q107 (2013).

[73] D. S. Meyaard, Q. Shan, Q. Dai, J. Cho, E. F. Schubert, M.-H. Kim, and C. Sone, "On the temperature dependence of electron leakage from the active region of GaInN/GaN light-emitting diodes," Appl. Phys. Lett. **99**(4), 041112 (2011).

[74] D. S. Meyaard, Q. Shan, J. Cho, E. Fred Schubert, S.-H. Han, M.-H. Kim, C. Sone, S. Jae Oh, and J. Kyu Kim, "Temperature dependent efficiency droop in GaInN light-emitting diodes with different current densities," Appl. Phys. Lett. **100**(8), 081106 (2012).

[75] J. H. Park, J. W. Lee, D. Y. Kim, J. Cho, E. F. Schubert, J. Kim, J. Lee, Y.-I. Kim, Y. Park, and J. K. Kim, "Variation of the external quantum efficiency with temperature and current density in red, blue, and deep ultraviolet light-emitting diodes," J. Appl. Phys. **119**(2), 023101 (2016).

[76] Y. Kawakami, Y. Narukawa, K. Omae, S. Fujita, and S. Nakamura, "Dimensionality of excitons in InGaN-based light emitting devices," Phys. Status Solidi A **178**(1), 331–336 (2000).

[77] A. K. Viswanath, J. I. Lee, S. T. Kim, G. M. Yang, H. J. Lee, and D. Kim, "Luminescence and ultrafast phenomena in InGaN multiple quantum wells," Thin Solid Films **515**(10), 4401–4404 (2007).

[78] S. P. Chang, J. R. Chang, K. P. Sou, Y. J. Li, Y. J. Cheng, H. C. Kuo, and C. Y. Chang, "Photoluminescent study of high indium content nanopyramid light emitting diodes," in *2013 Conference on Lasers and Electro-Optics Pacific Rim (CLEOPR), Kyoto, Japan, 30 June–4 July 2013* (IEEE, 2013).

[79] A. Schenk, "A model for the field and temperature dependence of Shockley-Read-Hall lifetimes in silicon," Solid State Electron. **35**(11), 1585–1596 (1992).

[80] J. I. Pankove, *Optical Processes in Semiconductors* (Prentice-Hall, 1971).

[81] C. H. Henry and D. V. Lang, "Nonradiative capture and recombination by multiphonon emission in GaAs and GaP," Phys. Rev. B **15**(2), 989–1016 (1977).

[82] Y. Shinozuka, "Electron-lattice interaction in nonmetallic materials: Configuration coordinate diagram and lattice relaxation," Jpn. J. Appl. Phys. **32**(Part 1, No. 10), 4560–4570 (1993).

[83] H. Goto, Y. Adachi, and T. Ikoma, "Carrier capture by multiphonon emission at extrinsic deep centers induced by self-trapping in GaAs," J. Appl. Phys. **54**(4), 1909–1923 (1983).

[84] W. R. Buchwald and N. M. Johnson, "Revised role for the Poole–Frenkel effect in deep-level characterization," J. Appl. Phys. **64**(2), 958–961 (1988).

[85] S. A. Lourenço, I. F. L. Dias, L. C. Poças, J. L. Duarte, J. B. B. de Oliveira, and J. C. Harmand, "Effect of temperature on the optical properties of GaAsSbN/GaAs single quantum wells grown by molecular-beam epitaxy," J. Appl. Phys. **93**(8), 4475–4479 (2003).

[86] J. D. Lambkin, L. Considine, S. Walsh, G. M. O'Connor, C. J. McDonagh, and T. J. Glynn, "Temperature dependence of the photoluminescence intensity of ordered and disordered $In_{0.48}Ga_{0.52}P$," Appl. Phys. Lett. **65**(1), 73–75 (1994).

[87]Y. Sun, Y.-H. Cho, H.-M. Kim, and T. W. Kang, "High efficiency and brightness of blue light emission from dislocation-free InGaN/GaN quantum well nanorod arrays," Appl. Phys. Lett. **87**(9), 093115 (2005).

[88]E. Rosencher and B. Vinter, *Optoelectronics* (Cambridge University Press, 2002).

[89]A. Haug, "Relations between the T_0 values of bulk and quantum-well GaAs," Appl. Phys. B **44**(3), 151–153 (1987).

[90]J. Hader, J. V. Moloney, and S. W. Koch, "Temperature-dependence of the internal efficiency droop in GaN-based diodes," Appl. Phys. Lett. **99**(18), 181127 (2011).

[91]N. K. Dutta, "Calculation of Auger rates in a quantum well structure and its application to InGaAsP quantum well lasers," J. Appl. Phys. **54**(3), 1236–1245 (1983).

[92]A. S. Polkovnikov and G. G. Zegrya, "Auger recombination in semiconductor quantum wells," Phys. Rev. B **58**(7), 4039–4056 (1998).

[93]A. Nirschl, A. Gomez-Iglesias, M. Sabathil, G. Hartung, J. Off, and D. Bougeard, "Quantitative modeling of the temperature-dependent internal quantum efficiency in InGaN light emitting diodes," Phys. Status Solidi A **211**(11), 2509–2513 (2014).

[94]F. Bertazzi, M. Goano, and E. Bellotti, "Numerical analysis of indirect Auger transitions in InGaN," Appl. Phys. Lett. **101**(1), 011111 (2012).

[95]E. Kioupakis, P. Rinke, K. T. Delaney, and C. G. Van de Walle, "Indirect Auger recombination as a cause of efficiency droop in nitride light-emitting diodes," Appl. Phys. Lett. **98**(16), 161107 (2011).

[96]K. W. Böer and U. W. Pohl, *Semiconductor Physics*, 1st ed. (Springer International Publishing, 2018).

[97]A. Laubsch, M. Sabathil, W. Bergbauer, M. Strassburg, H. Lugauer, M. Peter, S. Lutgen, N. Linder, K. Streubel, J. Hader, J. V. Moloney, B. Pasenow, and S. W. Koch, "On the origin of IQE-'droop' in InGaN LEDs," Phys. Status Solidi C **6**(S2), S913–S916 (2009).

[98]F. Bertazzi, X. Zhou, M. Goano, G. Ghione, and E. Bellotti, "Auger recombination in InGaN/GaN quantum wells: A full-Brillouin-zone study," Appl. Phys. Lett. **103**(8), 081106 (2013).

[99]R. Vaxenburg, A. Rodina, E. Lifshitz, and A. L. Efros, "The role of polarization fields in Auger-induced efficiency droop in nitride-based light-emitting diodes," Appl. Phys. Lett. **103**(22), 221111 (2013).

[100]R. Vaxenburg, E. Lifshitz, and A. L. Efros, "Suppression of Auger-stimulated efficiency droop in nitride-based light emitting diodes," Appl. Phys. Lett. **102**(3), 031120 (2013).

[101]T. Frost, A. Banerjee, S. Jahangir, and P. Bhattacharya, "Temperature-dependent measurement of Auger recombination in In 0.40 Ga 0.60 N/GaN red-emitting ($\lambda = 630$ nm) quantum dots," Appl. Phys. Lett. **104**(8), 081121 (2014).

[102]D. J. Myers, K. Gelžinytė, A. I. Alhassan, L. Martinelli, J. Peretti, S. Nakamura, C. Weisbuch, and J. S. Speck, "Direct measurement of hot-carrier generation in a semiconductor barrier heterostructure: Identification of the dominant mechanism for thermal droop," Phys. Rev. B **100**(12), 125303 (2019).

[103]G.-B. Lin, D. Meyaard, J. Cho, E. Fred Schubert, H. Shim, and C. Sone, "Analytic model for the efficiency droop in semiconductors with asymmetric carrier-transport properties based on drift-induced reduction of injection efficiency," Appl. Phys. Lett. **100**(16), 161106 (2012).

[104]C. De Santi, M. Meneghini, D. Monti, J. Glaab, M. Guttmann, J. Rass, S. Einfeldt, F. Mehnke, J. Enslin, T. Wernicke, M. Kneissl, G. Meneghesso, and E. Zanoni, "Recombination mechanisms and thermal droop in AlGaN-based UV-B LEDs," Photonics Res. **5**(2), A44–A51 (2017).

[105]A. Hori, D. Yasunaga, A. Satake, and K. Fujiwara, "Temperature dependence of electroluminescence intensity of green and blue InGaN single-quantum-well light-emitting diodes," Appl. Phys. Lett. **79**(22), 3723–3725 (2001).

[106]A. Hori, D. Yasunaga, A. Satake, and K. Fujiwara, "Temperature and current dependent capture of injected carriers in InGaN single-quantum-well light-emitting diodes," Phys. Status Solidi A **192**(1), 44–48 (2002).

[107]A. Hori, D. Yasunaga, A. Satake, and K. Fujiwara, "Temperature and injection current dependence of electroluminescence intensity in green and blue InGaN single-quantum-well light-emitting diodes," J. Appl. Phys. **93**(6), 3152–3157 (2003).

[108]P. Bakmiwewa, A. Hori, A. Satake, and K. Fujiwara, "Temperature-dependent electroluminescence anomalies influenced by injection current level in InGaN single-quantum-well diodes," Physica E **21**(2–4), 636–640 (2004).

[109]C. De Santi, M. Meneghini, A. Tibaldi, M. Vallone, M. Goano, F. Bertazzi, G. Verzellesi, G. Meneghesso, and E. Zanoni, *Physical Mechanisms Limiting the Performance and the Reliability of GaN-Based LEDs* (Elsevier, 2018), pp. 455–489.

[110]F. Bertazzi, M. Goano, G. Ghione, A. Tibaldi, P. Debernardi, and E. Bellotti, "Electron transport," in *Handbook of Optoelectronic Device Modeling and Simulation, Vol. 1*, edited by J. Piprek (CRC Press, Boca Raton, FL, 2017), Chap. 2, pp. 35–80.

[111]S. Chichibu, "Exciton localization in InGaN quantum well devices," J. Vac. Sci. Technol. B **16**(4), 2204 (1998).

[112]Y. Kawakami, K. Omae, A. Kaneta, K. Okamoto, Y. Narukawa, T. Mukai, and S. Fujita, "In inhomogeneity and emission characteristics of InGaN," J. Phys. Condens. Matter **13**(32), 6993–7010 (2001).

[113]Y. Estrin, D. H. Rich, S. Keller, and S. P. DenBaars, "Observations of exciton-surface plasmon polariton coupling and exciton-phonon coupling in InGaN/GaN quantum wells covered with Au, Ag, and Al films," J. Phys. Condens. Matter **27**(26), 265802 (2015).

[114]M. Leroux, N. Grandjean, M. Laügt, J. Massies, B. Gil, and P. Lefebvre, "Quantum confined Stark effect due to built-in internal polarization fields in (Al, Ga)N/GaN quantum wells," Phys. Rev. B **58**(20), R13371–R13374 (1998).

[115]Y.-H. Cho, G. H. Gainer, A. J. Fischer, J. J. Song, S. Keller, U. K. Mishra, and S. P. DenBaars, "'S-shaped' temperature-dependent emission shift and carrier dynamics in InGaN/GaN multiple quantum wells," Appl. Phys. Lett. **73**(10), 1370 (1998).

[116]F. Rossi, G. Salviati, M. Pavesi, M. Manfredi, M. Meneghini, G. Meneghesso, E. Zanoni, and U. Strauß, "Temperature and current dependence of the optical intensity and energy shift in blue InGaN-based light-emitting diodes: Comparison between electroluminescence and cathodoluminescence," Semicond. Sci. Technol. **21**(5), 638–642 (2006).

[117]X. A. Cao, S. F. LeBoeuf, L. B. Rowland, C. H. Yan, and H. Liu, "Temperature-dependent emission intensity and energy shift in InGaN/GaN multiple-quantum-well light-emitting diodes," Appl. Phys. Lett. **82**(21), 3614–3616 (2003).

[118]G. M. Wu, T. J. Chung, T. E. Nee, D. C. Kuo, W. J. Chen, C. C. Ke, C. W. Hung, J. C. Wang, and N. C. Chen, "Improvements of quantum efficiency and thermal stability by using Si delta doping in blue InGaN/GaN multiple quantum well light-emitting diodes," Phys. Status Solidi C **4**(7), 2797–2801 (2007).

[119]R. Jiang, H. Lu, D. J. Chen, F. F. Ren, D. W. Yan, R. Zhang, and Y. D. Zheng, "Temperature-dependent efficiency droop behaviors of GaN-based green light-emitting diodes," Chin. Phys. B **22**(4), 047805 (2013).

[120]J. Mickevičius, J. Jurkevičius, A. Kadys, G. Tamulaitis, M. Shur, M. Shatalov, J. Yang, and R. Gaska, "Temperature-dependent efficiency droop in AlGaN epitaxial layers and quantum wells," AIP Adv. **6**(4), 045212 (2016).

[121]J. D. Lambkin, D. J. Dunstan, K. P. Homewood, L. K. Howard, and M. T. Emeny, "Thermal quenching of the photoluminescence of InGaAs/GaAs and InGaAs/AlGaAs strained-layer quantum wells," Appl. Phys. Lett. **57**(19), 1986–1988 (1990).

[122]N. Otsuji, K. Fujiwara, and J. K. Sheu, "Electroluminescence efficiency of blue InGaN/GaN quantum-well diodes with and without an n-InGaN electron reservoir layer," J. Appl. Phys. **100**(11), 113105 (2006).

[123]S. Nakamura, M. Senoh, N. Iwasa, S. Nagahama, T. Yamada, and T. Mukai, "Superbright green InGaN single-quantum-well-structure light-emitting diodes," Jpn. J. Appl. Phys. **34**(Part 2, No. 10B), L1332–L1335 (1995).

[124]M. Calciati, M. Goano, F. Bertazzi, M. Vallone, X. Zhou, G. Ghione, M. Meneghini, G. Meneghesso, E. Zanoni, E. Bellotti, G. Verzellesi, D. Zhu, and C. Humphreys, "Correlating electroluminescence characterization and physics-based models of InGaN/GaN LEDs: Pitfalls and open issues," AIP Adv. **4**(6), 067118 (2014).

[125]F. Bernardini, V. Fiorentini, and D. Vanderbilt, "Spontaneous polarization and piezoelectric constants of III-V nitrides," Phys. Rev. B **56**(16), R10024–R10027 (1997).

[126]O. Ambacher, B. Foutz, J. Smart, J. R. Shealy, N. G. Weimann, K. Chu, M. Murphy, A. J. Sierakowski, W. J. Schaff, L. F. Eastman, R. Dimitrov, A. Mitchell, and M. Stutzmann, "Two dimensional electron gases induced by spontaneous and piezoelectric polarization in undoped and doped AlGaN/GaN heterostructures," J. Appl. Phys. **87**(1), 334–344 (2000).

[127]M. F. Schubert, J. Xu, J. K. Kim, E. F. Schubert, M. H. Kim, S. Yoon, S. M. Lee, C. Sone, T. Sakong, and Y. Park, "Polarization-matched GaInN/AlGaInN multi-quantum-well light-emitting diodes with reduced efficiency droop," Appl. Phys. Lett. **93**(4), 041102 (2008).

[128]D. Yan, L. Li, J. Ren, F. Wang, G. Yang, S. Xiao, and X. Gu, "Electron-leakage-related low-temperature light emission efficiency behavior in GaN-based blue light-emitting diodes," J. Semicond. **35**(4), 044007 (2014).

[129]G. Wachutka, "Consistent treatment of carrier emission and capture kinetics in electrothermal and energy transport models," Microelectron. J. **26**(2–3), 307–315 (1995).

[130]M. Lades, W. Kaindl, N. Kaminski, E. Niemann, and G. Wachutka, "Dynamics of incomplete ionized dopants and their impact on 4H/6H-SiC devices," IEEE Trans. Electron Devices **46**(3), 598–604 (1999).

[131]S. Chichibu, A. Shikanai, T. Azuhata, T. Sota, A. Kuramata, K. Horino, and S. Nakamura, "Effects of biaxial strain on exciton resonance energies of hexagonal GaN heteroepitaxial layers," Appl. Phys. Lett. **68**(26), 3766–3768 (1996).

[132]Y. Narukawa, Y. Kawakami, S. Fujita, S. Fujita, and S. Nakamura, "Recombination dynamics of localized excitons in In$_{0.20}$Ga$_{0.80}$N-In$_{0.05}$Ga$_{0.95}$N multiple quantum wells," Phys. Rev. B **55**(4), R1938–R1941 (1997).

[133]J. Binder, K. P. Korona, A. Wysmołek, M. Kamińska, K. Köhler, L. Kirste, O. Ambacher, M. Zaja¸c, and R. Dwiliński, "Dynamics of thermalization in GaInN/GaN quantum wells grown on ammonothermal GaN," J. Appl. Phys. **114**(22), 223504 (2013).

[134]P. G. Eliseev, P. Perlin, J. Lee, and M. Osiński, "'Blue' temperature-induced shift and band-tail emission in InGaN-based light sources," Appl. Phys. Lett. **71**(5), 569–571 (1997).

[135]O. H. Nam, K. H. Ha, J. S. Kwak, S. N. Lee, K. K. Choi, T. H. Chang, S. H. Chae, W. S. Lee, Y. J. Sung, H. S. Paek, J. H. Chae, T. Sakong, J. K. Son, H. Y. Ryu, Y. H. Kim, and Y. Park, "Characteristics of GaN-based laser diodes for post-DVD applications," Phys. Status Solidi A **201**(12), 2717–2720 (2004).

[136]C. H. Seager, S. M. Myers, A. F. Wright, D. D. Koleske, and A. A. Allerman, "Drift, diffusion, and trapping of hydrogen in p-type GaN," J. Appl. Phys. **92**(12), 7246–7252 (2002).

[137]C. De Santi, M. Meneghini, G. Meneghesso, and E. Zanoni, "Degradation of InGaN laser diodes caused by temperature- and current-driven diffusion processes," Microelectron. Reliab. **64**, 623–626 (2016).

[138]J. Glaab, J. Ruschel, T. Kolbe, A. Knauer, J. Rass, H. K. Cho, N. Lobo Ploch, S. Kreutzmann, S. Einfeldt, M. Weyers, and M. Kneissl, "Degradation of (In)AlGaN-based UVB LEDs and migration of hydrogen," IEEE Photonics Technol. Lett. **31**(7), 529–532 (2019).

[139]M. Leroux, N. Grandjean, B. Beaumont, G. Nataf, F. Semond, J. Massies, and P. Gibart, "Temperature quenching of photoluminescence intensities in undoped and doped GaN," J. Appl. Phys. **86**(7), 3721–3728 (1999).

[140]C. De Santi, M. Meneghini, M. La Grassa, B. Galler, R. Zeisel, M. Goano, S. Dominici, M. Mandurrino, F. Bertazzi, D. Robidas, G. Meneghesso, and E. Zanoni, "Role of defects in the thermal droop of InGaN-based light emitting diodes," J. Appl. Phys. **119**(9), 094501 (2016).

[141]D. Schiavon, M. Binder, M. Peter, B. Galler, P. Drechsel, and F. Scholz, "Wavelength-dependent determination of the recombination rate coefficients in single-quantum-well GaInN/GaN light emitting diodes," Phys. Status Solidi B **250**(2), 283–290 (2013).

[142]C. Huh and S.-J. Park, "Effects of temperature on InGaN/GaN LEDs with different MQW structures," Electrochem. Solid State Lett. **7**(11), G266 (2004).

[143]K. T. Lam and S. J. Chang, "GaN-based LEDs with hot/cold factor improved by the electron blocking layer," J. Disp. Technol. **10**(12), 1078–1082 (2014).

[144]K. S. Kim, J. H. Kim, S. J. Jung, Y. J. Park, and S. N. Cho, "Stable temperature characteristics of InGaN blue light emitting diodes using AlGaN/GaN/InGaN superlattices as electron blocking layer," Appl. Phys. Lett. **96**, 091104 (2010).

[145]H. Schneider and K. V. Klitzing, "Thermionic emission and Gaussian transport of holes in a GaAs/Al$_x$Ga$_{1-x}$As multiple-quantum-well structure," Phys. Rev. B **38**(9), 6160–6165 (1988).

[146]J. R. Lang, N. G. Young, R. M. Farrell, Y.-R. Wu, and J. S. Speck, "Carrier escape mechanism dependence on barrier thickness and temperature in InGaN quantum well solar cells," Appl. Phys. Lett. **101**(18), 181105 (2012).

[147]D. Pons and S. Makram-Ebeid, "Phonon assisted tunnel emission of electrons from deep levels in GaAs," J. Phys. Fr. **40**(12), 1161–1172 (1979).

[148]D. M. Sathaiya and S. Karmalkar, "Thermionic trap-assisted tunneling model and its application to leakage current in nitrided oxides and AlGaN/GaN high electron mobility transistors," J. Appl. Phys. **99**, 093701 (2006).

[149]D. M. Sathaiya and S. Karmalkar, "A closed-form model for thermionic trap-assisted tunneling," IEEE Trans. Electron Devices **55**(2), 557–564 (2008).

[150]M. Auf der Maur, B. Galler, I. Pietzonka, M. Strassburg, H. Lugauer, and A. Di Carlo, "Trap-assisted tunneling in InGaN/GaN single-quantum-well light-emitting diodes," Appl. Phys. Lett. **105**(13), 133504 (2014).

[151]C. De Santi, M. Buffolo, N. Renso, A. Neviani, G. Meneghesso, E. Zanoni, and M. Meneghini, "Evidence for defect-assisted tunneling and recombination at extremely low current in InGaN/GaN-based LEDs," Appl. Phys. Express **12**(5), 052007 (2019).

[152]S. M. Sze, *Physics of Semiconductor Devices*, 2nd ed. (John Wiley & Sons, New York, 1981).

[153]W.-A. Quitsch, D. Sager, M. Loewenich, T. Meyer, B. Hahn, and G. Bacher, "Low injection losses in InGaN/GaN LEDs: The correlation of photoluminescence, electroluminescence, and photocurrent measurements," J. Appl. Phys. **123**(21), 214502 (2018).

[154]M. Meneghini, L.-R. Trevisanello, G. Meneghesso, and E. Zanoni, "A review on the reliability of GaN-based LEDs," IEEE Trans. Device Mater. Reliab. **8**(2), 323–331 (2008).

[155]P. Kamyczek, E. Placzek-Popko, V. Kolkovsky, S. Grzanka, and R. Czernecki, "A deep acceptor defect responsible for the yellow luminescence in GaN and AlGaN," J. Appl. Phys. **111**, 113105 (2012).

[156]J. Neugebauer and C. G. Van de Walle, "Gallium vacancies and the yellow luminescence in GaN," Appl. Phys. Lett. **69**(4), 503–505 (1996).

[157]A. Sedhain, J. Li, J. Y. Lin, and H. X. Jiang, "Nature of deep center emissions in GaN," Appl. Phys. Lett. **96**(15), 151902 (2010).

[158]T. Ogino and M. Aoki, "Mechanism of yellow luminescence in GaN," Jpn. J. Appl. Phys. **19**(12), 2395–2405 (1980).

[159]J. L. Lyons, A. Janotti, and C. G. Van de Walle, "Carbon impurities and the yellow luminescence in GaN," Appl. Phys. Lett. **97**(15), 152108 (2010).

[160]M. A. Reshchikov and H. Morkoç, "Luminescence properties of defects in GaN," J. Appl. Phys. **97**(6), 061301 (2005).

[161]X. Li and J. J. Coleman, "Time-dependent study of low energy electron beam irradiation of Mg-doped GaN grown by metalorganic chemical vapor deposition," Appl. Phys. Lett. **69**(11), 1605 (1996).

[162]A. Y. Polyakov and I.-H. Lee, "Deep traps in GaN-based structures as affecting the performance of GaN devices," Mater. Sci. Eng. R Rep. **94**, 1–56 (2015).

[163]F. Mehnke, C. Kuhn, J. Stellmach, T. Kolbe, N. Lobo-Ploch, J. Rass, M.-A. Rothe, C. Reich, N. Ledentsov, M. Pristovsek, T. Wernicke, and M. Kneissl, "Effect of heterostructure design on carrier injection and emission characteristics of 295 nm light emitting diodes," J. Appl. Phys. **117**(19), 195704 (2015).

[164]J. Rass, T. Kolbe, N. Lobo-Ploch, T. Wernicke, F. Mehnke, C. Kuhn, J. Enslin, M. Guttmann, C. Reich, A. Mogilatenko, J. Glaab, C. Stoelmacker, M. Lapeyrade, S. Einfeldt, M. Weyers, and M. Kneissl, "High-power UV-B LEDs with long lifetime," Proc. SPIE **9363**, 93631K (2015).

[165]M. Lapeyrade, A. Muhin, S. Einfeldt, U. Zeimer, A. Mogilatenko, M. Weyers, and M. Kneissl, "Electrical properties and microstructure of vanadium-based contacts on ICP plasma etched n-type AlGaN:Si and GaN:Si surfaces," Semicond. Sci. Technol. **28**(12), 125015 (2013).

[166]G. Steude, B. K. Meyer, A. Göldner, A. Hoffmann, F. Bertram, J. Christen, H. Amano, and I. Akasaki, "Optical investigations of AlGaN on GaN epitaxial films," Appl. Phys. Lett. **74**(17), 2456–2458 (1999).

[167]N. Nepal, J. Li, M. L. Nakarmi, J. Y. Lin, and H. X. Jiang, "Exciton localization in AlGaN alloys," Appl. Phys. Lett. **88**(6), 062103 (2006).

[168]H. Murotani, Y. Yamada, T. Taguchi, A. Ishibashi, Y. Kawaguchi, and T. Yokogawa, "Temperature dependence of localized exciton transitions in AlGaN ternary alloy epitaxial layers," J. Appl. Phys. **104**(5), 053514 (2008).

[169]Y. Iwata, T. Oto, D. Gachet, R. G. Banal, M. Funato, and Y. Kawakami, "Co-existence of a few and sub micron inhomogeneities in Al-rich AlGaN/AlN quantum wells," J. Appl. Phys. **117**(11), 115702 (2015).

[170]H. X. Jiang and J. Y. Lin, "AlGaN and InAlGaN alloys—Epitaxial growth, optical and electrical properties, and applications," Opto-Electron. Rev. **10**(4), 271–286 (2002).

[171]S. Nakamura, "The roles of structural imperfections in InGaN-based blue light-emitting diodes and laser diodes," Science **281**(5379), 956–961 (1998).

[172]Figure from commercially-available LED datasheet: Cree XLamp XP-E.

[173]See http://dm.henkel-dam.com/is/content/henkel/274-Henkel Bergquist LED Thermal Solutionspdf for "Henkel Bergquist selection guide: thermal management for LED."

[174]Y. Xi and E. F. Schubert, "Junction–temperature measurement in GaN ultraviolet light-emitting diodes using diode forward voltage method," Appl. Phys. Lett. **85**(12), 2163–2165 (2004).

[175]S. Chhajed, Y. Xi, T. Gessmann, J.-Q. Xi, J. M. Shah, J. K. Kim, and E. F. Schubert, "Junction temperature in light-emitting diodes assessed by different methods," Proc SPIE **5739**, 16 (2005).